Utjecaj trodimenzionalnih polimernih nanostruktura na razvoj primarnih živčanih stanica

Miloš, Frano

Master's thesis / Diplomski rad

2017

Permanent link / Trajna poveznica: <https://urn.nsk.hr/urn:nbn:hr:217:965770>

Download date / Datum preuzimanja: **2024-04-19**

Repository / Repozitorij:

[Repository of the Faculty of Science - University of Zagreb](#)

University of Zagreb

Faculty of Science

Department of Biology

Frano Miloš

Influence of three-dimensional polymeric nanostructures on the development of primary neurons

Utjecaj trodimenzionalnih polimernih nanostruktura na razvoj primarnih živčanih stanica

Graduation thesis

Zagreb, 2017.

TEMELJNA DOKUMENTACIJSKA KARTICA

Utjecaj trodimenzionalnih polimernih nanostruktura na razvoj primarnih živčanih stanica

Frano Miloš

Rooseveltov trg 6, 10000 Zagreb, Hrvatska

Površine sa specifičnom topografijom imaju potencijal u poboljšanju sučelja između stanica i biomedicinskih uređaja poput neuralnih implantata i biosenzora te bi mogle omogućiti liječenje različitih neuroloških poremećaja – sljepoće, paralize, Parkinsonove bolesti. Napredak nanotehnologije omogućio je izradu supstrata s točno definiranim mehaničkim i morfološkim svojstvima. Topografija izvanstaničnog okoliša utječe na staničnu morfologiju i razvoj te se može koristiti za kontroliranje stanične adhezije i diferencijacije. Cilj ovog rada je istražiti utjecaj površinske topografije na razvoj primarnih živčanih stanica. Primarne živčane stanice su izolirane iz korteksa mozga embrija štakora te kultivirane na supstratima polimera OrmoComp s nano- i mikrostupovima. Supstrati od polimera OrmoComp su podržavali rast živčanih stanica te nisu imali štetan utjecaj na njihovu vijabilnost. Nano- i mikrostupovi su poticali usmjereni rast živčanih stanica te njihovo poravnanje s topografijom pri čemu je ovaj efekt bio manje izražen kod stupova s većim promjerom i većim međusobnim razmakom. Pritom je povećanje visine stupova povećalo efekt usmjerenog rasta aksona te rezultiralo dužim i pravilnije raspoređenim aksonima. Osim toga, aksoni na topografijama su istraživali veći prostor tijekom rasta te su rasli brže i efikasnije što je rezultiralo povećanjem njihove duljine. Ovaj rad pokazuje da supstrati polimera OrmoComp s nano- i mikrostupovima podržavaju i kontroliraju rast kortikalnih živčanih stanica. Također, povećani i usmjereni rast aksona pokazuje potencijal ovih supstrata u regeneraciji oštećenog živčanog tkiva.

BASIC DOCUMENTATION CARD

University of Zagreb

Faculty of Science

Department of Biology   Graduation Thesis

Influence of three-dimensional polymeric nanostructures on the development of primary neurons

Frano Miloš

Rooseveltov trg 6, 10000 Zagreb, Croatia

Surfaces with a defined topography could improve the interface between cells and biomedical devices such as neural implants and biosensors and enable treatment of various neurological disorders – blindness, paralysis, Parkinson's disease. Advances in nanofabrication technologies have allowed generation of substrates with defined mechanical and morphological properties. Topography of the extracellular environment affects cell morphology and development and can be used to control adhesion and differentiation. The aim of this thesis was to investigate the influence of topography on the development of embryonic cortical neurons. Cortical neurons isolated from rat embryos were cultured on OrmoComp polymer substrates with nano- and micropillars. OrmoComp substrates supported neuronal growth without detrimental effects on cell viability. Nano- and microscale pillars enhanced neurite growth and alignment to the topography, an effect that diminished with increasing pillar diameter and spacing. Moreover, an increase in pillar height largely enhanced the axon guiding effect resulting in longer and more aligned axons. Live cell imaging revealed that axons growing on different topographies explored a larger area and had a more rapid and directional growth which resulted in an increase in axon length. This study demonstrates the suitability of OrmoComp nano- and micropillar substrates for supporting and controlling growth of cortical neurons. Furthermore, enhanced axon elongation and topographical guidance demonstrate the potential of these substrates as tissue engineering scaffolds for regeneration of damaged nerves.

ABBREVIATIONS

ECM	Extracellular matrix
CNS	Central nervous system
PNS	Peripheral nervous system
min	Minute
sec	Second
h	Hour
P	Peripheral
C	Central
T	Transition
MT	Microtubule
FA	Focal adhesion
DIV	Days *in vitro*
EBL	Electron-beam litography
RIE	Reactive-ion etching
NIL	Nanoimprint litography
PMMA	Polymethylmethacrylat
2D	Two-dimensional
3D	Three-dimensional
slm	Standard liters per minute
sccm	Standard cubic centimetres
rpm	Revolutions per minute
RT	Room temperature
PLL	Poly-L Lysine
HBSS	Hanks Balanced Salt Solution
RPMI	Roswell Park Memorial Institute
sCMOS	Scientific complementary metal-oxide-semiconductor
BB	Blocking buffer

TABLE OF CONTENT

1. INTRODUCTION

The extracellular environment consists of different physical and biochemical cues influencing cell functions and behavior. The relationship between topography and neuronal development has long been studied in order to make the *in vitro* environment of neuronal cultures similar to *in vivo* conditions. Neuronal cells are embedded in an intricate network of proteins and polysaccharides called the extracellular matrix (ECM). In this complex microenvironment, the crosstalk between distinct biochemical, structural, and mechanical stimuli affects different aspects of cell behavior including morphogenesis and differentiation (Joo et al. 2015; Ma et al. 2008). The ECM proteins form complex structures ranging from micrometers to nanometers in size, which represent the topography of the ECM. Since cells possess nanoscale features compatible with those of the ECM (e.g., filopodia), its architecture exerts an influence over cellular development, differentiation and neuritogenesis by providing contact guidance cues (Provenzano et al. 2008).

Advances in the fields of micro- and nanotechnology have allowed the fabrication of substrates with precisely defined mechanical and morphological properties. Because the size of their features is of the same order of magnitude as the structures formed by biomolecules, these materials are valuable tools for nanoscale manipulation of living systems *in vitro*. The ability to control cellular development would advance our understanding of basic cellular processes and enable the control of cellular migration, proliferation, and differentiation. Artificial substrates with a defined surface architecture are highly relevant in biomedical research of neural implants and biosensors which promise new treatments of various neurological disorders – blindness, epilepsy, paralysis, Parkinson's disease (Hatsopoulos and Donoghue 2009). Currently, the cell-device interfaces are fabricated from different materials and investigation into their interaction with living cells and tissues is of paramount importance in developing a new generation of functional and biocompatible neural implants. Such nanostructured implants would interact conformally with the tissue evoking less of an immune response. The aim of this thesis is to investigate the influence of surface topography on the development and morphology of primary neuronal cells.

1.1. The nervous system

The nervous system is an intricate network of nerves and specialized neuronal cells that coordinate and transmit signals to and from the body. It can be divided into two parts: the central nervous system (CNS) and the peripheral nervous system (PNS), which together control the body and enable communication with its environment. The CNS consists of the brain and the spinal cord that integrate, process and coordinate conscious and subconscious sensory information coming from the body. It is connected to every other part of the body through a complex network of sensory neurons, ganglia (clusters of neurons) and nerves (enclosed bundles of axons) which form the PNS. The PNS transmits signals from the environment and other parts of the body to the brain and the spinal cord via sensory nerves where they are processed and transmitted via the motor nerves to the organs of the body.

The brain is the most complex part of the nervous system that regulates both the unconscious processes, such as digestion and breathing, and higher functions such as language, creativity, expression, emotions, and personality. The human brain weighs on average about 1.2-1.4 kg and is composed of approximately 100 billion neurons. These form a vastly complex network of about 100 trillion synapses (Kandel et al. 2000). The largest part of the brain is the cerebrum located above the cerebellum and the brain stem. The outer region of the cerebrum is the cerebral cortex, which is a convoluted 2-4 mm thick layer of gray matter. The bulges of the cortex are called gyri while the indentations are called sulci. These greatly increase the cortical surface area in the confined volume of the skull. The many functional areas of the cortex are associated with perception, attention, awareness, memory, thought, and language. In recent years, there have been many attempts to design functioning neural implants that would be able to interface directly with specific areas of the cortex. These devices could stimulate functional areas of the cortex and circumvent damaged neural circuitry thus potentially providing treatment for disorders such as blindness, deafness, dementia (Konrad and Shanks 2010). Therefore, it is important to make the cell-device interface biomimetic i.e. make it as similar as possible to *in vivo* environments to improve functionality and avoid an immune response.

1.2. Neuronal cells

The ability of the brain to carry out complex tasks is due to the structural and functional properties of interconnected neurons. Although similar to other cells in the body, neuronal cells are specialized to receive, integrate, and transmit electrical or chemical signals throughout the body. These functions are reflected in and made possible by their anatomy. A typical neuronal cell has four distinct parts: the cell body (or soma), dendrites, and an axon with axon terminals (Figure 1.1.). The soma contains the nucleus and represents the metabolic center of the neuron producing all the proteins for dendrites, axons and synaptic terminals. Neuronal processes (neurites) conduct signals to or from the soma with incoming signals being received by the dendrites and outgoing signals transmitted through the axon. Some axons are covered with myelin produced by supporting glial cells, which acts as an insulator to minimize dissipation of the electrical signal as it travels down the axon, greatly increasing the speed of conduction (Martini 2004). The signal propagates to the axon terminals that connect neurons through a chemical synapse. The electrical signal in the form of an action potential triggers the release of neurotransmitters from the presynaptic cell. These then cross the synapse and bind to membrane receptors on the postsynaptic cell. When the neurotransmitter binds the receptor on the surface of the postsynaptic cell, the electrochemical potential of the target cell changes, and the next electrical impulse is launched, conveying an excitatory or inhibitory signal. A single neuron can receive inputs from many presynaptic neurons and it can also make synaptic connections on numerous postsynaptic neurons via different axon terminals. Thus, neuronal morphology varies from simple cells with one extending neurite to highly complex cells with a myriad of neurites and thousands of synapses.
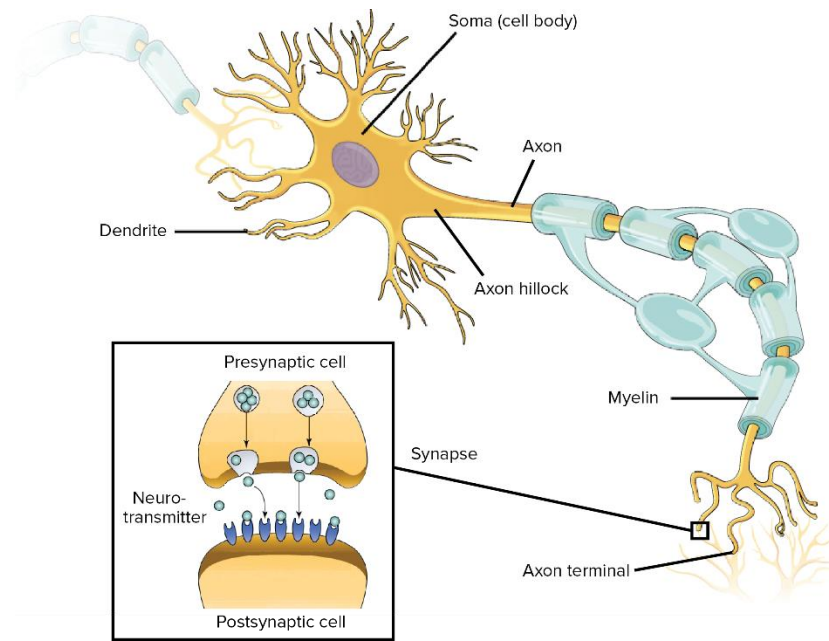
Figure 1.1. Structure of a neuronal cell. *A neuron consists of a cell body (soma), dendrites, and an axon ending in axon terminals that are connected to neighboring neurons through a chemical synapse. Figure adapted from OpenStax College, Biology (www.cnx.org).*

1.2.1. Neuronal development

The incredible morphological diversity of neurons is due to developing neurons extending long and branching neurites from the soma. During embryogenesis, neurons mature from the outermost cell layer of the embryo, the ectoderm, through a process called neurogenesis. In the presented thesis, immature neuronal cells are isolated from the rat embryo cortex. After settling and adhering to the substrate, they sprout many thin filopodia (Figure 1.2., Stage 1). Subsequently, immature neurites are formed (Stage 2) that extend through several cycles of growth and retraction (Dotti et al. 1988), resulting in a symmetrical morphology of the cell. Neurites are extended via a growth cone, a highly motile enlargement at the tip of the neurite. After approximately 12 hours in culture, one neurite starts growing rapidly and breaks the overall symmetry (Jacobson et al. 2006), becoming the axon (Stage 3). The remaining neurons mature into dendrites, which subsequently develop Y-shaped branches resulting in complex dendritic trees (Stage 4). Lastly, dendritic spines are formed facilitating the connections between neighboring cells (Stage 5).
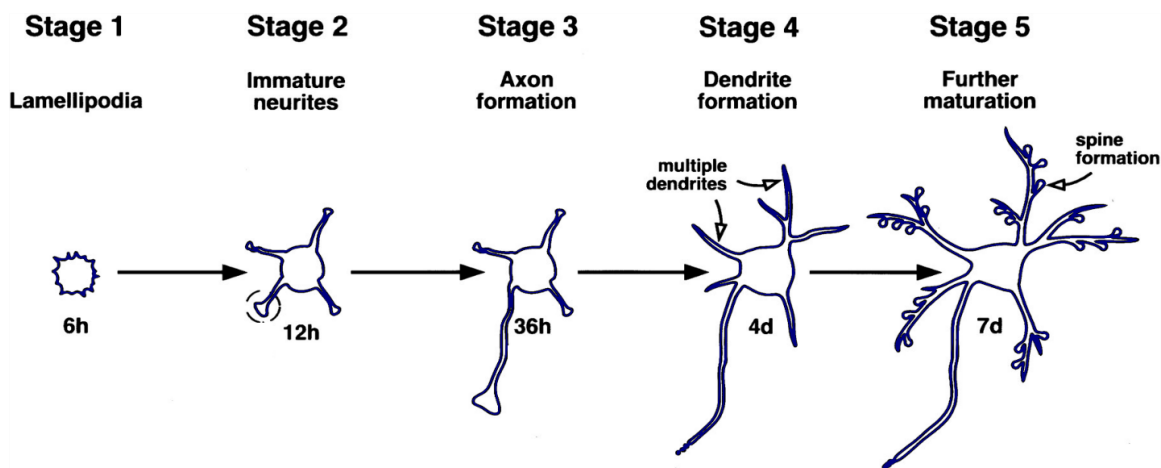
Figure 1.2. A schematic representation of neuronal development. *Several hours after seeding, neurons form a lamellipodium with many thin filopodia (Stage 1) which develop into neurites (Stage 2). Eventually, one neurite breaks the symmetry and extends rapidly becoming an axon (Stage 3). The remaining neurites mature and branch into dendrites creating a dendritic tree (Stage 4). After a week, dendritic spines are formed and synaptic contacts are established (Stage 5). Figure adapted from Govek et al. 2005.*

1.3. Axonal growth

Neurons must elongate their axons during development to create functional networks and properly wire the nervous system together. Our understanding of how this happens, i.e. how axons elongate at a particular rate and then stop at the proper time, is still rather limited. Axons are usually 1 μm thick and can be more than 1 m long (Martini 2004). The growth of such massive structures requires many processes occurring simultaneously – membrane and cytoplasmic element production, their transportation to the growing axon and the coordination of these events with the growth cone's exploration of its surroundings through advancing, retracting, pausing, or turning (Goldberg 2003). In the following sections, the microscopic details of axonal growth will be addressed, followed by an overview of the underlying molecular mechanisms.

1.3.1. The growth cone

The growth cone is a highly dynamic tip of the axon involved in elongation and pathfinding. Axon pathfinding is responsible both for establishing neuronal networks in the developing brain (Bernhardt 1999), and for the re-wiring of damaged pathways due to injury or disease (Becker and Becker 2007). Growth cone and axon guidance are important in investigating neuronal response to topography and controlling axon guidance, which could lead to new treatments of nerve damage (Geller and Fawcett 2002). Growth cones can be characterized by fine cylindrical extensions called filopodia, containing bundles of actin filaments, receptors and cell adhesion molecules that are important for axon growth and guidance. Flat regions of dense actin meshwork between the filopodia are called lamellipodia (Figure 1.3.A).

The growth cone has three domains with different types of cytoskeletal filaments (Dent and Gertler 2003): a central (C) domain containing microtubules (MTs), an actin-rich peripheral (P) domain, and a transitional (T) domain between the central and peripheral domains (Figure 1.3.B). Through persistent protrusion and withdrawal of filopodia and lamellipodia from the P-domain, the growth cone detects local adhesive ligands and extrinsic guidance cues. Most filopodia range from 5 to 20 µm in length, while a small fraction can reach even 50 µm, suggesting that growth cones can explore large swaths of their surroundings (Letourneau 1979; Hammarback and Letourneau 1986). Filopodia and lamellipodia are protruded and withdrawn at rates of 1–4 µm/min (Gomez and Letourneau 2014).
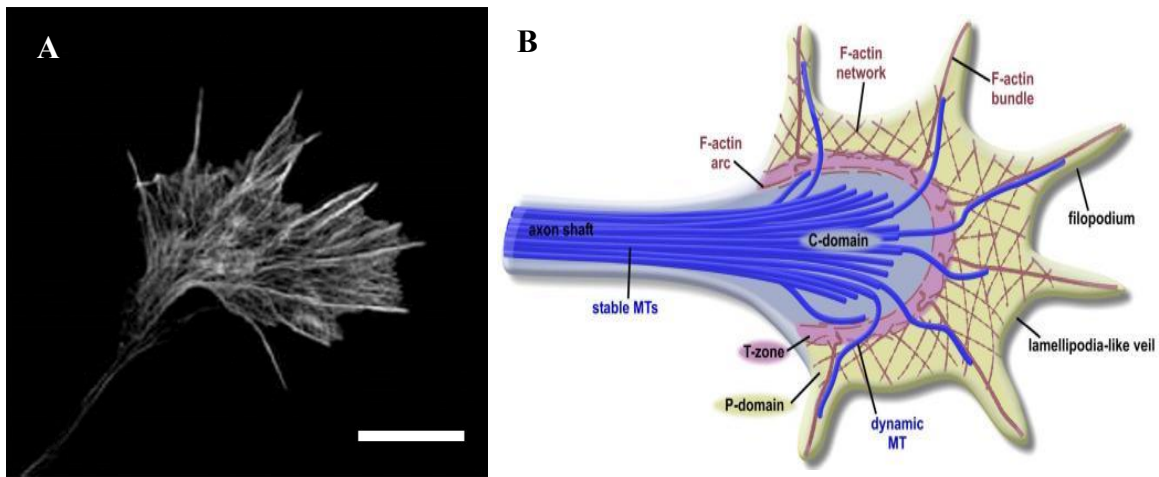
Figure 1.3. The growth cone. A) *A fluorescent image of a mouse hippocampal growth cone labeled with fluorescent phalloidin. F-actin is concentrated in filopodia (bundles) and lamellipodia (meshwork). Scale bar: 5 µm.* ***B)*** *A schematic representation of the growth cone structure. The dynamic filopodia at the leading edge explore the surroundings. They are separated by sheets of membrane called lamellipodia. The P-domain contains long actin bundles, which form the filopodia and mesh-like branched F-actin networks. The C-domain encloses stable, bundled microtubules (MTs) that enter the growth cone, numerous organelles, vesicles, and actin bundles. Dynamic MTs from the C-domain can enter the P-domain moving along F-actin bundles. Finally, the T-domain at the interface between the P- and C-domains contains contractile actin arcs interacting with myosin that lie perpendicular to F-actin bundles. Figures adapted from Lowery and Van Vactor 2009.*

The growth cone continuously goes through three stages of advance: protrusion, engorgement and consolidation (Dent and Gertler 2003). Protruding filopodia extend rapidly along the leading edge of the growth cone and eventually move to the lateral sides. During engorgement, microtubules invade further into the growth cone, bringing vesicles and organelles. Finally, F-actin at the neck of the growth cone depolymerizes and the filopodia retract (consolidation). The membrane then shrinks to form a cylindrical axon shaft around the bundle of microtubules.

Growth cone motility and filopodia protrusion are driven primarily by the cyclical polymerization and depolymerization of actin filaments. Actin filaments in the P-domain are continuously assembled at the leading edge, which elongates the tips of lamellipodia and filopodia and pushes the growth cone membrane forward. Meanwhile, the actin filaments are pushed away from the leading edge by a myosin-motor driven process (Forscher and Smith 1988; Mitchison and Cramer 1996). Actin polymerization at the leading edge and myosin-driven contraction of actin filaments toward C-domain generate a net retrograde flow of the actin network relative to the direction of axon elongation. In the central domain, retrograde flow prevents the microtubules from invading the peripheral domain, thus blocking its advance and axon elongation (Forscher and Smith 1988). When the rate of the anterograde polymerization and retrograde flow and depolymerization is the same, the growth cone neither advances nor retracts. During protrusion, actin polymerization exceeds retrograde flow and actin depolymerization while during retraction retrograde flow and F-actin breakdown exceed actin polymerization at the leading edge.

The growth cone motility is mediated by binding of integrin receptors to the ECM which leads to the formation of contact adhesion complexes. These are related to focal adhesions although much less is understood about their molecular regulation and function. Integrins are αβ-heterodimers with a large extracellular domain that binds the ECM proteins (fibronectin, laminin, collagen I) and a short cytoplasmic tail that links to the actin cytoskeleton (Hynes 2002). Integrins also bind cell surface receptors of the immunoglobulin superfamily (ICAM -1, VCAM-1). Actin filaments inside the cells continuously search for suitable attachment sites and, when they reach a precursor contact, they are stabilized by additional integrins, actin filaments and other proteins such as vinculin and talin. The resulting complex is known as a point contact in neuronal cells which acts as a molecular clutch by mediating transient interactions between the moving actin cytoskeleton and ECM-bound integrins (Mitchison and Kirschner 1988, Figure 1.4.). Point contact adhesions usually assemble within filopodia that contain parallel bundled actin, have a short lifetime, and then disassemble near the base of filopodia. The anchoring of actin filaments slows the retrograde flow, which permits the advance of microtubules and promotes axonal elongation.
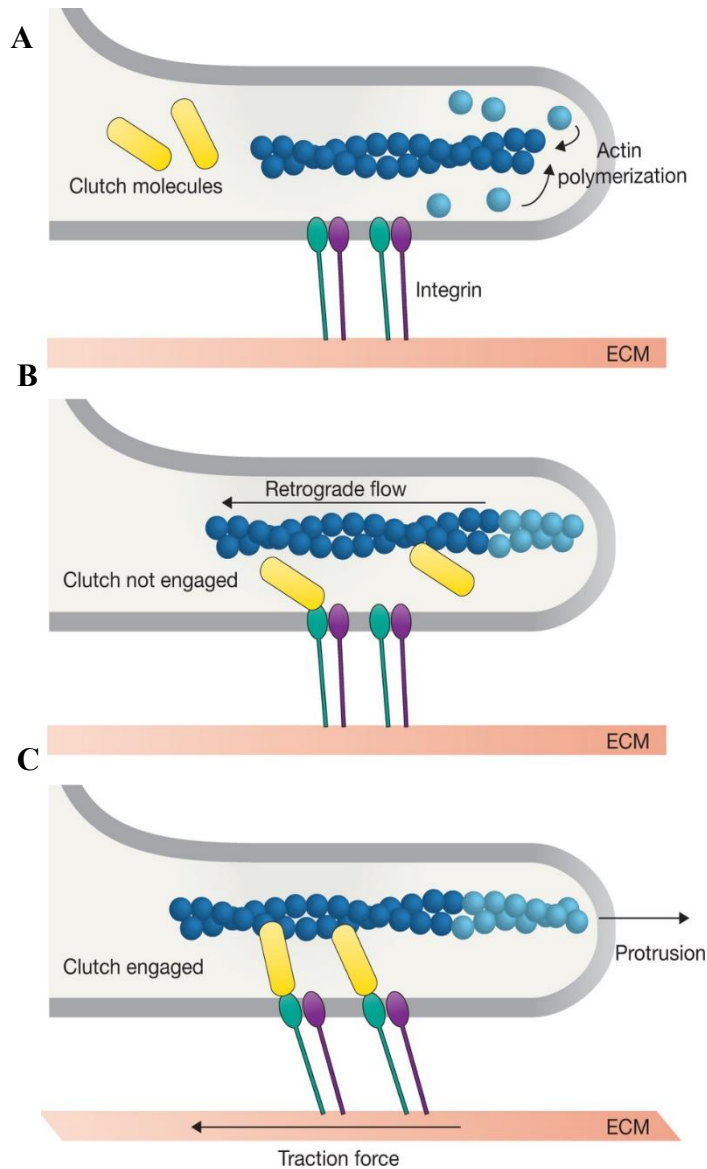
Figure 1.4. The molecular clutch model. A) *New actin monomers (light blue) are incorporated into a pre-existing actin filament at the leading edge (dark blue). Transmembrane integrin dimers (green and purple) are bound to the extracellular matrix (red).* ***B)*** *When the clutch is not engaged to connect actin filaments to the ECM, actin polymerization results in rapid retrograde cytoskeletal flow with no net leading edge protrusion, and no traction force on the ECM.* ***C)*** *If the clutch is engaged (yellow), the forces generated by polymerization of the actin cytoskeleton are transmitted to the ECM, which slows the retrograde flow resulting in the generation of traction force on the ECM, and a net edge protrusion. Figure adapted from Case and Waterman 2015.*

1.3.2. Focal adhesions

Since the performance of implantable devices, biosensors, and micro-electrode arrays depends on how cells interact with the device surface, nanofabrication techniques are used to improve their biocompatibility and promote cell adhesion (Ma 2008; Chen et al. 2005). The investigation of the interface between cells and the surface topography is important for designing and improving these devices and implants. Focal adhesions (FAs) are integrin-based structures that connect the actin cytoskeleton to the ECM (Figure 1.5., Chen et al. 2003). They reduce the gap between the cell membrane and the substrate surface to only 10-15 nm, as compared to the normal gap of more than 50 nm (Zaidel-Bar et al. 2004).

FAs are dynamic structures, through which mechanical force and regulatory signals are transmitted between the cell and ECM. They can contain hundreds of different proteins including scaffold proteins, structural proteins, kinases, and phosphatases, and their composition changes in response to diverse stimuli. Nascent adhesions are initiated by the binding of actin filaments to integrins via adaptor proteins like talin, α-actinin, filamin, vinculin, tensin and intracellular signaling proteins, such as focal adhesion kinase (Zamir and Geiger 2001). Most of these nascent FAs have a lifetime of ~1 min but some undergo further stabilization and maturation during which they elongate in the direction of retrograde flow (Choi et al. 2008). The development of the initial adhesion into a focal complex is marked by the recruitment of vinculin (Humphries et al. 2007). As vinculin is recruited and the focal complex is formed, there is a decrease in the distance between the adhesion and the surface to form a "tight" or "focal" junction (Izzard 1988). Focal complexes can continue to mature into large, stable focal adhesions, extending further from the cell periphery (Riveline et al. 2001). This reinforces the linkage to actin by recruitment of additional scaffolding and signaling components. Although a complete mechanism of the formation and maturation of FAs in response to mechanical stimuli is unknown, it is proposed that integrin receptors activate signaling pathways in response to extracellular mechanical forces thereby converting physical cues to biochemical signals (Wang et al. 2005). While the existence of FAs in neurons has not been proven, smaller point contacts are present in almost all adherent cells.
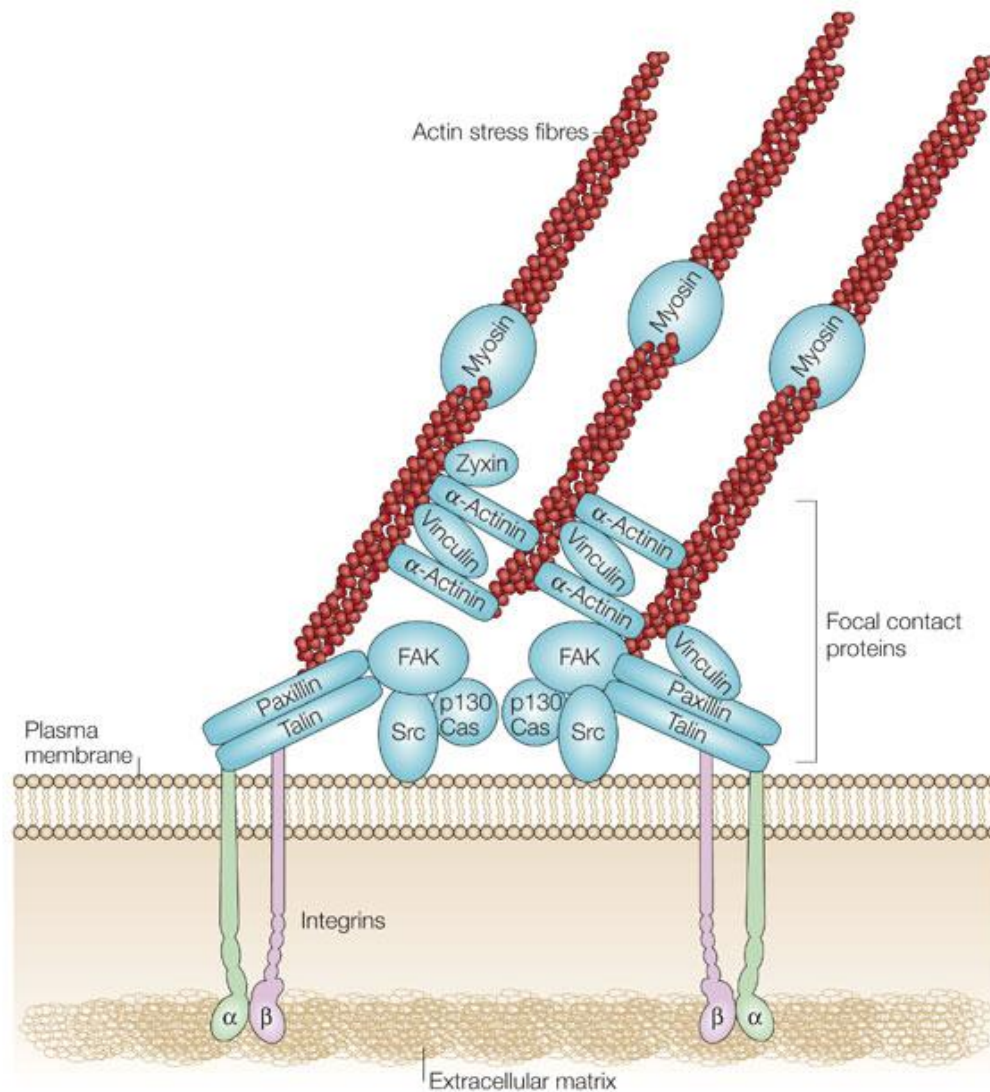
Figure 1.5. Key components of focal adhesions. *Integrin receptors bind to ECM proteins, such as collagen, laminin, and fibronectin and recruit scaffolding proteins, such as talin, paxillin, and vinculin. Focal adhesion kinase (FAK) and Src kinase modulate the adhesions through phosphorylation, which allows assembly of additional proteins. Several proteins bind directly to actin filaments (red), which restrains the retrograde flow and allows the force of actin polymerization to generate membrane protrusions. Figure adapted from Mitra et al. 2005.*

1.4. Contact guidance

During neurogenesis, immature neurons must extend their axons to a specific site to create functional networks and eventually establish the nervous system. The patterning of neuronal connections emerges from precise and coordinated interactions between developing axons and their environment. Growth cones are highly responsive to multiple sources of complex cues which can be non-diffusible, short range and diffusible, or long range (Tessier-Lavigne and Goodman 1996). The former involves integrin-mediated binding to molecules presented on a neighboring cell surface (transmembrane cell adhesion molecules) or those assembled into the ECM (laminin, fibronectin). On the other hand, anti-adhesive surface-bound molecules (slits, ephrins) can restrict growth cone advance (Chilton 2006). Long range chemotropic cues include morphogens (Zou and Lyuksyutova 2007), secreted transcription factors (Butler and Tear 2007), neurotrophic factors and neurotransmitters (Sanford et al. 2008). Axons, intended for different sites, respond to cues in diverse ways, i.e. they are attracted or repelled.

Contact guidance is a phenomenon named by Paul Weiss in 1945 and first observed by R. G. Harrison in 1911, when he reported that solid material can influence cell morphology and movement describing the adaptation of movement and shape in cells growing on a spider web (Harrison 1912). Contact guidance has a particular role in the development of the nervous system. For example, radial glial cells guide cortical neurons during histogenesis of the cortex, acting as a scaffold and a source of new neurons (Rakic 1972; Nadarajah et al. 2002). In addition, neurons in the medulla oblongata were found to migrate parallel to oriented glial tracts, which play a crucial role in establishing proper connectivity (Ono and Kawamura 1989). Moreover, rather than simply serving as a scaffold for neuronal development and axon pathfinding, glial tracts may provide both biochemical and physical cues that are vital to ensuring the establishment of proper connectivity.

Additionally, contact guidance plays a role in the response to injury. Schwann cells aid in the repair of injuries in the PNS by producing growth factors, cleaning up debris caused by axon degeneration, and laying down tracks along which the regenerating axon can extend (Bunge 1994). On the other hand, injuries in the CNS are incapable of spontaneous repair due to the formation of physical and chemical barriers and a lack of a prompt immune response (Avellino et al. 1995).

Recent advances in micro- and nanofabrication techniques have propelled numerous studies into contact guidance using different artificial substrates consisting of biochemical and/or

topographical cues. Controlling cell development and behavior topography can prove advantageous for tissue engineering such as grafts for nerves or tendons, implants, biosensors, and micro-electrode arrays. Several studies have demonstrated that surface topography can promote neuronal regeneration (Repić et al. 2016; Cho et al. 2010). In addition to creating ordered neural networks, topography can be used to improve the cell-electrode interface thereby promoting both recording and electrical stimulation of neurons cultured on micro-electrode arrays (Keefer et al. 2008).

1.5. Nanotechnology

Recent developments in nanofabrication techniques have enabled precise tuning of mechanical and morphological properties of surfaces and their use in the investigation of nanomaterial interactions with living systems *in vitro*. There are two general approaches to nanostructure fabrication: the "bottom-up" and the "top-down" approaches (Biswas et al. 2012). In the former, the nanostructures are created by placing atoms or molecules one at a time to build the desired nanostructure while the latter entails sculpting the desired structures from a bulk material using different etching procedures. All structures in the presented thesis have been fabricated using the "top-down" approach. The fabrication of micro- and nanometer sized structures involves specific techniques including electron beam lithography, reactive ion etching and nanoimprint lithography, which will be described in subsequent sections.

1.5.1. Electron-beam lithography

Electron-beam lithography (EBL) is a technique based on chemically modifying an electron-sensitive resist using a focused beam of electrons (Chen 2015). The resist, coated onto a silicon wafer, is sensitive to irradiation, upon which it becomes either more soluble (positive resist) or less soluble (negative resist). A pattern is defined by illuminating certain areas and then chemically removing the soluble parts of the resist layer. Although, the pattern created in the resist itself can be used, usually the silicon wafer under the resist is etched with chemicals or an ion gas (reactive ion etching – RIE). In the presented thesis, polymethylmethacrylate (PMMA) was used as a resist for EBL. The pattern in the resist was not used as a mold directly since PMMA is very porous so

that organic solvents or monomers easily penetrate into it which causes regional surface inhomogeneity in the resist composition and consequently leads to swelling of the mold. This has a serious effect on reproducibility due to degradation during repeated patterning. The resist that remains after EBL protects the wafer so that etching will only affect the exposed parts of the wafer. This resist is removed after the process. The main advantage of EBL is the fabrication of patterns with sub-10 nm resolution. However, due to its low throughput, its use is limited to research purposes and low-volume production of semiconductor devices.

1.5.2. Reactive-ion etching

Reactive ion etching (RIE) is a directional etching method that uses chemically reactive plasma to etch substrates (Fluitman 1996). The plasma is generated by an electromagnetic field under vacuum, creating high-energy ions that bombard the wafer surface and react with it. The reactive species are chosen for their ability to react chemically with the material being etched. Therefore, RIE is a synergistic process between chemically active species and energetic ion bombardment. Since the ion bombardment is directional, RIE can be designed to be highly anisotropic, meaning it is essential when narrow lines or channels are needed or when high aspect ratio structures need to be fabricated.

1.5.3. Nanoimprint lithography

With the use of materials with micro- and nanotopographies becoming ever more prevalent in both basic and applied research, the lack of low-cost and high-throughput manufacturing technologies has been a major bottleneck in this field. Nanoimprint lithography (NIL) was first described by Chou et al. (1996) and has since become a preferred method since it does not require clean room facilities and expensive machines once the master mold has been fabricated. A master mold with nanostructures on its surface is pressed into a thin layer of polymer under high pressure and temperature, replicating the nanostructures on the mold in the polymer. This procedure can be repeated several times creating many polymer replicas from a single master mold with the choice of polymer being almost arbitrary. Therefore, the main advantage of this technique is the ability to pattern sub-25 nm structures over a large area with a high-throughput and low-cost.

1.6. Cell response to artificial topographies

Although, many fundamental principles in cell biology have been studied on flat two-dimensional (2D) rigid substrates, these hardly recapitulate the complexity of *in vivo* microenvironments that influence cell function and behavior (Cukierman et al. 2001; Yamada and Cukierman 2017). Advances in the fields of micro- and nanotechnology have enabled fabrication of substrates that mimic certain features of the *in vivo* environment while still maintaining the simplicity of traditional 2D *in vitro* systems. Micro- and nanostructured surfaces are produced either by spatially distributing biomolecules (chemical patterning) or by modifying the surface into micro- and nanotopographies (topographic patterning). Although, substrate topography is a nonbiological way to affect cell behavior, it has biomimetic features imitating those in the *in vivo* environment. Microengineered substrates have been used extensively to study the impact of the ECM microenvironment on cell development and functions. However, since basement membranes of tissues possess various nanoscale features (5-500 nm), nanotopography may be more biomimetic than microtopography (Flemming et al. 1999). More recently, the attention has been focused on the investigation of the ECM nanotopography (Bettinger et al. 2009; Kshitiz et al. 2015) which strongly influences cellular polarity, migration, proliferation and differentiation. In these studies, the nanotopography was modelled in form of different arrays containing parallel nanogrooves, nanoridges, nanopillars/holes, fibers, etc., (Figure 1.6.). These substrates provide different guidance cues and strongly influence cell behavior through contact guidance (Clark et al. 1991). In general, the various substrates used can be classified in two groups – isotropic and anisotropic topographies.
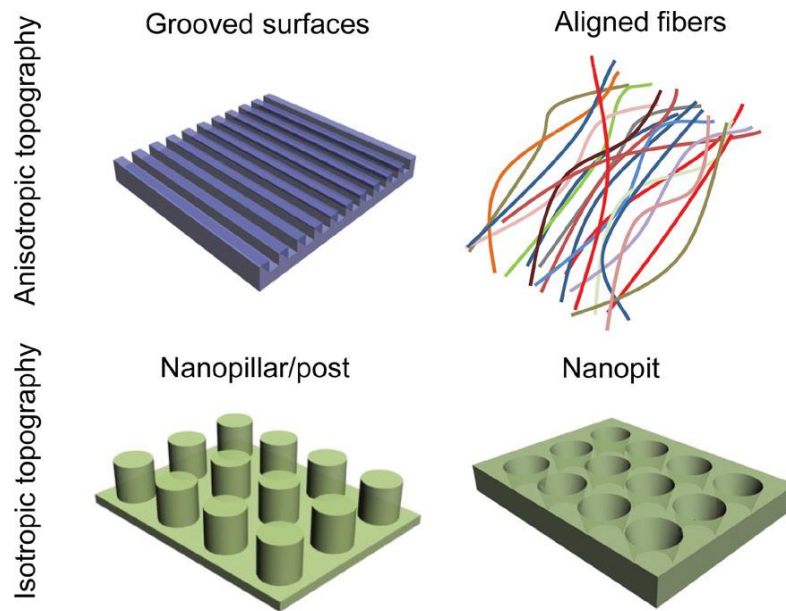
Figure 1.6. Artificial nanotopographies. *Representative nanotopographies commonly used as cell culture substrates include anisotropic and isotropic topographies. Anisotropic topographies (nanogrooves/ridges, aligned fibers) are directionally dependent, providing cues along a single direction while isotropic topographies provide cues along multiple directions (nanopillars/posts, nanoholes). Figure adapted from Kim et al. 2012.*

The cell response to different surfaces depends not only on its topography but also on the material and type of cells used. For example, glioblastoma multiforme cancer cells display different responses when cultured on nanochannel surfaces than normal fibroblast cells (Ning et al. 2016). Although, both cell lines survive and proliferate on the nanostructured surface, glioblastomas are softer, spread to a larger area, and elongate less than fibroblasts. Neurons create extensive networks of neurites that extend from the soma and exhibit various responses to the surrounding topography. One of the most interesting responses is the neurite alignment to the imposed topography (Figure 1.7.B, C) as opposed to a random orientation of neurites on un-patterned surfaces (Figure 1.7.A), which has potential in neural tissue engineering (Bellamkonda 2006). Additionally, a range of other effects have been reported including reduced number of neurites (Yao et al. 2009), increased neurite length (Lietz et al. 2006), and increased polarization (Foley et al. 2005).

1.6.1. Isotropic topographies

Uniformly or randomly textured surfaces containing nodes, pits, protrusions, pillars, and channels, influence complex cell functions. These topographies may provide guideposts at discrete locations resulting in a distinct response to features with different dimensions. Studies with dimensions less than 5 μm have shown that cells, regardless of type, exhibit a smaller, rounded morphology with less organized cytoskeletons (Martinez et al. 2009). Neurons, due to their unique morphology, exhibit distinct responses on isotropic topographies. Several studies have shown that neurites follow interrupted guidance cues with a high degree of fidelity (Figure 1.7.B). Dowell-Mesfin et al. (2004) used surfaces with 1 μm tall pillars either 0.5 or 2 μm in diameter and arranged in a grid with 1.5 to 4.5 μm spacing and demonstrated that hippocampal neurons align to pillar geometries, moving between adjacent pillars. The neurites tended to span the smallest distance between pillars, aligning either at 0° or 90°, with the highest alignment when pillars were large and with the smallest spacing. As the spacing increased, the fidelity of alignment decreased with 4.5 μm spacing resulting in a completely random distribution of neurites, similar to that found on a flat surface. Furthermore, neurons at DIV 1 on the pillar topographies had a single presumed axon forming, indicating a changed functional state of neurons caused by the topography. This is contrast to the model of neuronal development on flat surfaces (Figure 1.2.) where axon formation and extension occur approximately after 2 DIV. In a similar study, hippocampal neurons were plated on surfaces with posts 10-100 μm in diameter and edge to edge spacing of 10-200 μm (Hanson et al. 2009)) with the height of each post being approximately one tenth of the diameter. Neurons exhibited neurite alignment on surfaces with smaller features and smaller spacings, mostly following a single direction but occasionally branching in the perpendicular direction. However, the increase in feature diameters lead to neurites circling around the post with spacing of 20 μm, promoting both random outgrowth and circling. Therefore, isotropic topographies aligned neurites that tended to follow what contact they already had and "jumping" to a new contact only if it was in close enough proximity.

Cho et al. (2010) observed an accelerated neurite outgrowth of hippocampal neurons growing on anodized aluminum oxide (AAO) substrates with different feature dimensions. Substrates with a pitch of 400 nm accelerated neuronal polarization, while those with a very small pitch (63 nm) had no effect on polarization or neurite outgrowth. A separate study also reported a pitch-dependent

acceleration of neurite outgrowth using silica beads (Kang et al. 2012). Accelerated neurite outgrowth was observed on beads with dimensions larger than 200 nm and this effect disappeared after biochemical inhibition of filopodia formation with cytochalasin D, an actin-disrupting agent. This implies that neurons sense nanotopographies through filopodia, which in turn modulated intracellular cytoskeletal dynamics. These studies suggest that neuritogenesis is highly dependent on the pitch of the features presented on the substrate.

1.6.2. Anisotropic topographies

Anisotropic topographies have long been used to study and control cell migration and orientation (Figure 1.7.C). Nagata et al. (2006) have shown that neurons in the PNS polarize along nanogrooves designed to imitate neurite bundles suggesting that the topography of neurite bundles may regulate the polarity of neuronal cells. These studies have shown that both cells and their cytoskeleton display directional organization along the presented topography (Wojciak-Stothard et al. 1995). Moreover, the orientation of actin filaments and microtubules was identified as the primary event in cell alignment (den Braber et al. 1998), along with the localization of focal adhesion proteins such as vinculin (Wojciak-Stothard et al. 1996). Generally, alignment increases with increasing height/depth of the topography while it decreases with increasing width and pitch (Walboomers et al. 1999). Studies with microgrooves and ridges with depth increasing from around 0.2 to 4 μm have indicated an increase in neurite alignment and outgrowth on large structures, with no effect being observed on feature sizes less than 200 nm (Hirono et al. 1988; Walsh et al. 2005).

Recent studies have focused on whether cells align on nanoscale ridges and grooves and, if so, how small the features can be to still induce contact guidance. Teixeira et al. (2003) showed that the alignment of corneal epithelial cells varied with the dimensions of the nanoscale topography (depth and pitch). Cells aligned on ridges as small as 70 nm wide (400 nm pitch, 600 nm deep groove). Groove depth (150-600 nm) affected cell alignment more than pattern pitch (400–4000 nm). Furthermore, aligned axonal elongation was reported on 100 to 400 nm wide nanoimprinted grooves (300 nm deep) where the cell processes preferentially grew on ridge edges and elevations rather than in grooves (Johansson et al. 2006).

Although, the majority of studies using grooved substrates report parallel alignment of neuronal cell bodies and neurites, it has been demonstrated that submicron grooves can elicit perpendicular contact guidance in CNS neuroblasts (Nagata et al. 1993) and rat hippocampal cells (Rajnicek et al. 1997). Neurites crossed over adjacent grooves and ridges rather than extend parallel to a single feature making this an interesting phenomenon since cells and cellular processes usually tend to conform to wide and shallow grooves, while they span narrow and deep grooves (Martinez et al. 2009). Chua et al. (2014) proposed a model suggesting that increasing the depth of the grooves means that a growing neurite has to bend more to reach the surface. Therefore, an increase in height likely imposes a higher energetic cost on microtubule reorganization which means that it cannot conform to the groove and instead extended across it. This phenomenon has been reported *in vivo* (Ono et al. 1997), and in 2D, 3D, microexplant and organotypic cerebellar cultures (Nagata et al. 2006).
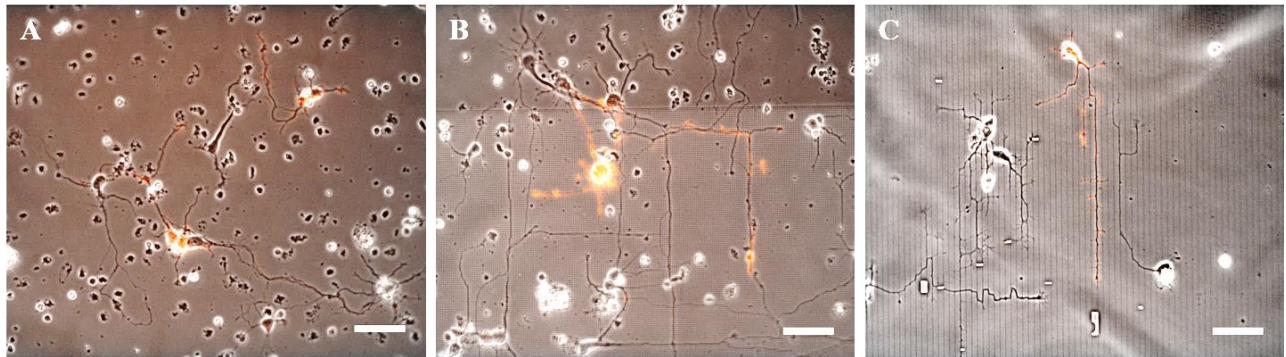
Figure 1.7. Cortical neurons growing on artificial nanotopographies. Cortical neurons used in this work are shown on an A) a flat surface, B) an isotropic array with nanopillars (400 nm in height, 750 nm in diameter and 1.5 µm pitch), C) anisotropic array with nanopillars (250 nm diameter, 100 nm height) ordered in lines with 250 nm interpillar pitch and 5 µm interline pitch. Cells are expressing a fluorescent actin marker (Lifeact RFP). Scale bars: 50 µm.

1.7. Mechanisms of cellular responses to topography

Although numerous studies have investigated the influence of topography on cell behavior the underlying mechanisms by which cells sense the topography remain unknown. Initial theories dealt

with the mechanical properties of the cytoskeleton and how they influence the likelihood that actin filaments would polymerize in a certain direction. These models assume that cytoskeletal elements are unable to bend more than a few degrees and if they encounter sharp edges they extend along the edge, or stay on the planar surface (Dunn and Brown 1986).

More recent models involve the probability of focal adhesion formation at certain sites. These propose that ECM proteins preferentially bind the discontinuities in the topography and, through integrin mediated binding and focal adhesion formation, lead to contact guidance (den Braber et al. 1996; Meyle et al. 1993). Nanopatterning techniques have provided valuable insights into focal adhesion signaling. Dalby et al. (2004) demonstrated that fibroblasts seeded on nanocolumnar substrates have larger filopodia and the increased surface contact guided cell migration by regulating the strength of focal adhesions through focal adhesion kinase and myosin II (Frey et al. 2006). Li et al. (2005) showed that aligned fibers promote actin polymerization and protrusion parallel to the fibers which can result in aligned focal adhesions and traction force through the actin cytoskeleton in the same direction. Larger focal adhesions, aligned actin fibers, polarized morphology, and enhanced motility have been observed in NIH-3T3 cells growing on nanoporous substrates (Nasrollahi et al. 2016), Furthermore, Gerecht et al. (2007) showed that the addition of actin-disrupting agents prevents the alignment of human embryonic stem cells in response to nanotopography. Taken together, these reports demonstrate that contact guidance is mediated by an interplay between adhesion signaling, the actin cytoskeleton, and substrate interactions.

Therefore, EBL and NIL are suitable techniques for designing and fabricating specific topographies to study and control cell behavior and development. The presented work applied these principles to cortical neurons isolated from rat embryos to study their development on different surfaces in order to determine optimal strategies for improving micro-electrode arrays and advancing neural implants and tissue engineering methods. It is presented that these surfaces promoted neurite outgrowth and provided guidance cues for growing axons, responses similar to those discussed in section 1.6.1.

2. MATERIALS AND METHODS

This chapter will present the methods applied in this thesis. Firstly, substrate preparation procedures including a brief description of fabrication processes will be presented. Subsequent sections will focus on neuronal cell culture, time-lapse microscopy and fluorescent immunocytochemistry. Finally, statistical methods used in the presented thesis will be described.

2.1. Substrate preparation

All substrates were fabricated in a controlled environment with a very low number of contaminants such as dust, aerosol particles, and chemical vapors (class 100 clean room). The fabrication of Si/SiO$_2$ molds and OrmoComp replicas was done by Andreea Belu (Belu 2017, PhD thesis).

2.1.1. Fabrication of Si/SiO$_2$ molds

Si/SiO$_2$ molds were fabricated from 4-inch silica wafers (n-type, 500-550 µm thickness, <100> crystal orientation, 2-10 Ωcm volume resistivity, Si-Mat company) using a top-down approach. A wafer was oxidized to produce a layer of SiO$_2$ using dry oxidation at 6 slm O$_2$ and 1100°C for 60 min in Centrotherm CLV 200 oxidation chamber (Figure 2.1.A). A layer of polymethylmethacrylate resist (PMMA, AR-P 669.04, Allresist) was deposited homogeneously on the wafer using spin coating (3000 rpm for 45 sec) and baked at 180°C for 5 min (Figure 2.1.B). Nanopatterns were designed using CleWin software (CleWin 4) and transferred onto PMMA resist using electron beam lithography (EBL, EBPG 5000plus from Vistec B.V., now Raith B.V.). The resist was exposed to a beam size 5 nm, 2 nA beam current, 50 kV voltage with different doses to create patterns. The labels were created with a 50 nm beam, 150 nA beam current, and 250 µC/cm^2 dose (Figure 2.1.C). The wafers were then immersed in developer AR600-55 (Allresist) for 2 min to remove small, more soluble PMMA fragments created by the electron beam and dipped in isopropanol (Sigma-Aldrich) for another 2 min to stop the developer effect (Figure 2.1.D). Finally, nanoholes of specified dimensions were etched into the exposed SiO$_2$ using reactive ion etching (RIE, Oxford Instruments). The recipe used was CH$_3$/SF$_6$ (10/50 sccm) plasma chemistry which

provides a sufficiently high selectivity etching over the resist (Figure 2.1.E). The rest of the PMMA layer was etched in the RIE chamber using O_2 plasma for 90 sec (Figure 2.1.F).
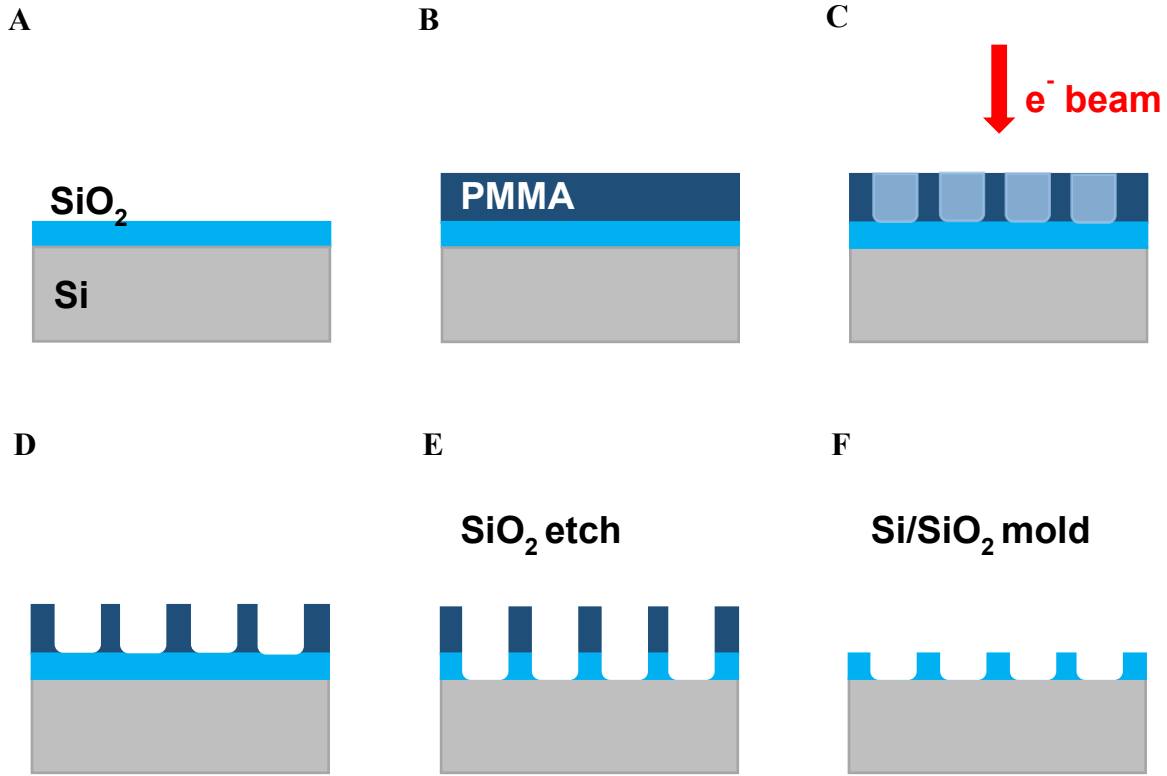
***Figure 2.1. Fabrication of nanostructured Si/SiO₂ molds. A)** A Si wafer is oxidized to produce SiO₂ layer. **B)** Wafer is coated with a PMMA resist. **C)** Electron-beam lithography creates the designed nanopattern in the PMMA. **D)** During development, PMMA fragments created by EBL are removed. **E)** SiO₂ is etched using reactive ion etching. **F)** Excess PMMA is etched away to create a nanostructured Si/SiO₂ mold.*

2.1.2. Surface modification of molds

The mold surface was passivated to facilitate its removal after the replication process. First, the molds were cleaned and activated using O_2 plasma (Plasma Surface Technology Pico-Diener electronic) for 2 min at 200 W and 1.4 mbar to enable silanization. The contact angle after activation was below 10° which means that the surface was hydrophilic. The wafers were then

transferred to an argon atmosphere glove box (99.99% argon, MBraun) for silanization. Trichloro(1H,1H,2H,2H-perfluorooctyl)silane (FOTCS, 40 µl evaporate to the gas phase) was deposited at 45 mbar for 1.5 h. The FOTCS molecules interact covalently with -OH groups on the surface, which increases the surface hydrophobicity thereby inducing a repellent behavior. Finally, the wafers were reintroduced in the clean room and rinsed in acetone, isopropanol and water cascade before replication.

2.1.3. Fabrication of OrmoComp replicas

OrmoComp polymer was deposited on quartz 4-inch wafers (525 ± 10 µm thickness, Plan Optics AG). First, the quartz wafers were dehydrated for at least 10 min at 200°C. An adhesive promoter, OrmoPrime, was deposited using spinning at 4000 rpm for 45 sec and baked for 5 min at 150°C to promote polymer adhesion. Wafers were then coated with the OrmoComp solution (OrmoComp:OrmoThin = 1:12) at 4000 rpm for 45 sec and baked at 80°C for 2 min. The quartz/OrmoComp replicas were produced using nanoimprint lithography (NIL, NX-2000, Nanonex Corp). The mold and the quartz/OrmoComp wafer were placed together between two films and compressed (Figure 2.2.). The process lasted 5 min at 500 psi (34.5 bar), followed by 1 min of UV curing (365 nm of emitted light wavelength) at RT. The wafers were separated with blades and isopropanol which reduces adhesion. Finally, the quartz/OrmoComp replicas were hard baked in an oven at 150°C for 16 h.
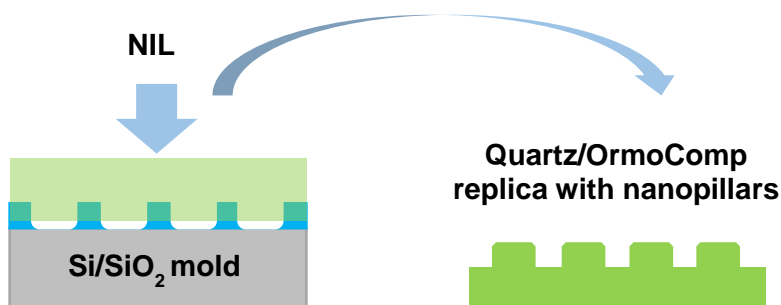
Figure 2.2. Fabrication of nanostructured quartz/OrmoComp replicas. A quartz/OrmoComp replica is compressed onto a Si/SiO$_2$ mold using nanoimprint lithography to fabricate a polymer substrate with nanopillars.

2.1.4. Design and characterization of topographies

Topographies used in this thesis consisted of nanostructures of defined dimensions uniformly ordered in all directions over the entire area (isotropically). Isotropic arrays can be characterized by the diameter (D) of the pillars, their depth (molds) or height (polymer replicas) and the pitch (P), i.e., distance between the centers of the top surface of two neighboring pillars (Figure 2.3.).
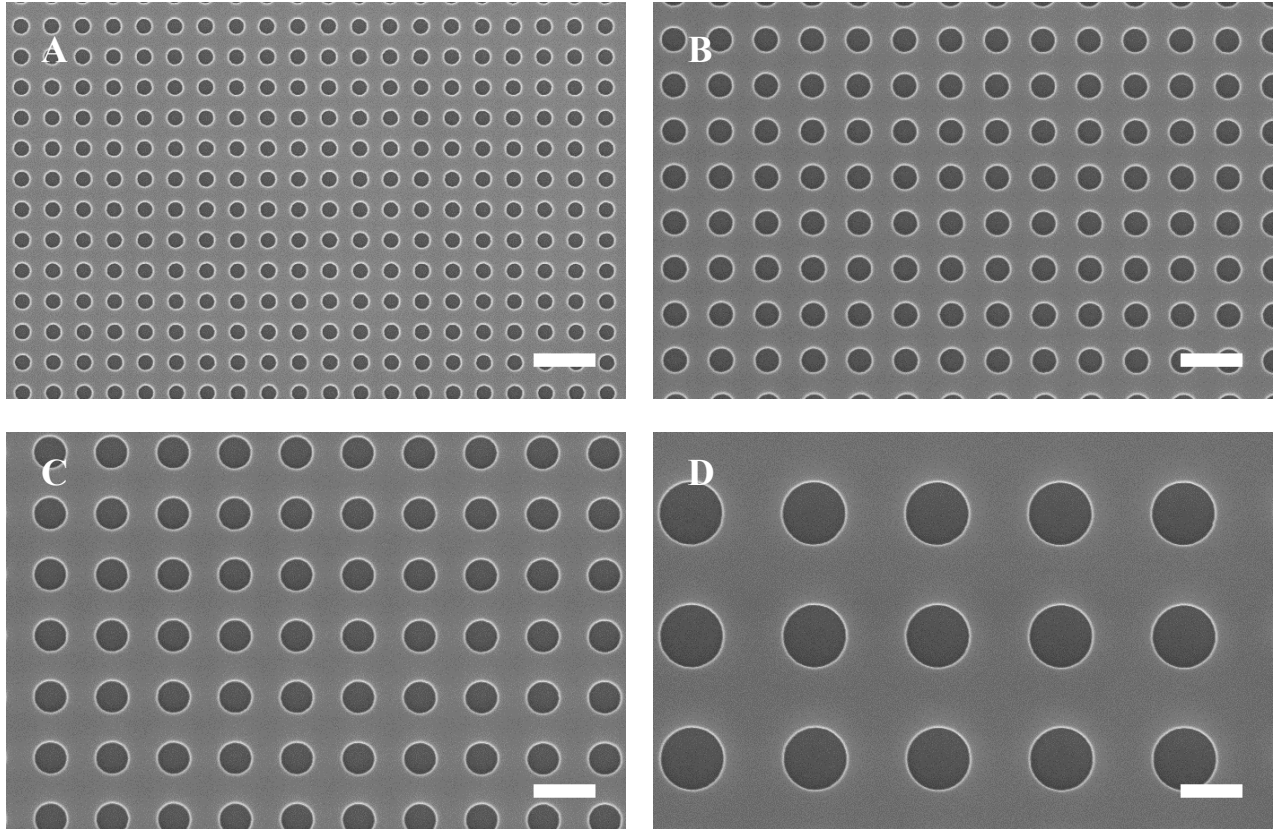
***Figure 2.3. SEM images of four isotropic array molds. A**) D = 0.5 µm, P = 1 µm (A0.5). **B)** D = 0.75 µm, P = 1.5 µm (A0.75). **C)** D = 1 µm, P = 2 µm (A1). **D)** D = 2 µm, P = 4 µm (A2). All structures are 100 nm in depth. Scale bars: 2 µm*

Si/SiO$_2$ molds were replicated in the OrmoComp hybrid polymer which is suitable for nanoimprint lithography due to its good reproducibility and low cost (Schizas and Karalekas 2011). OrmoComp has attracted attention for microfabrication applications in biomedicine and tissue engineering due to its biocompatibility. Molds with both 100 nm (Figure 2.4.A) and 400 nm (Figure 2.4.C) depth

were replicated resulting in polymer replicas with nanopillars of 100 nm (Figure 2.4.B) and 400 nm (Figure 2.4.D) in height, respectively.
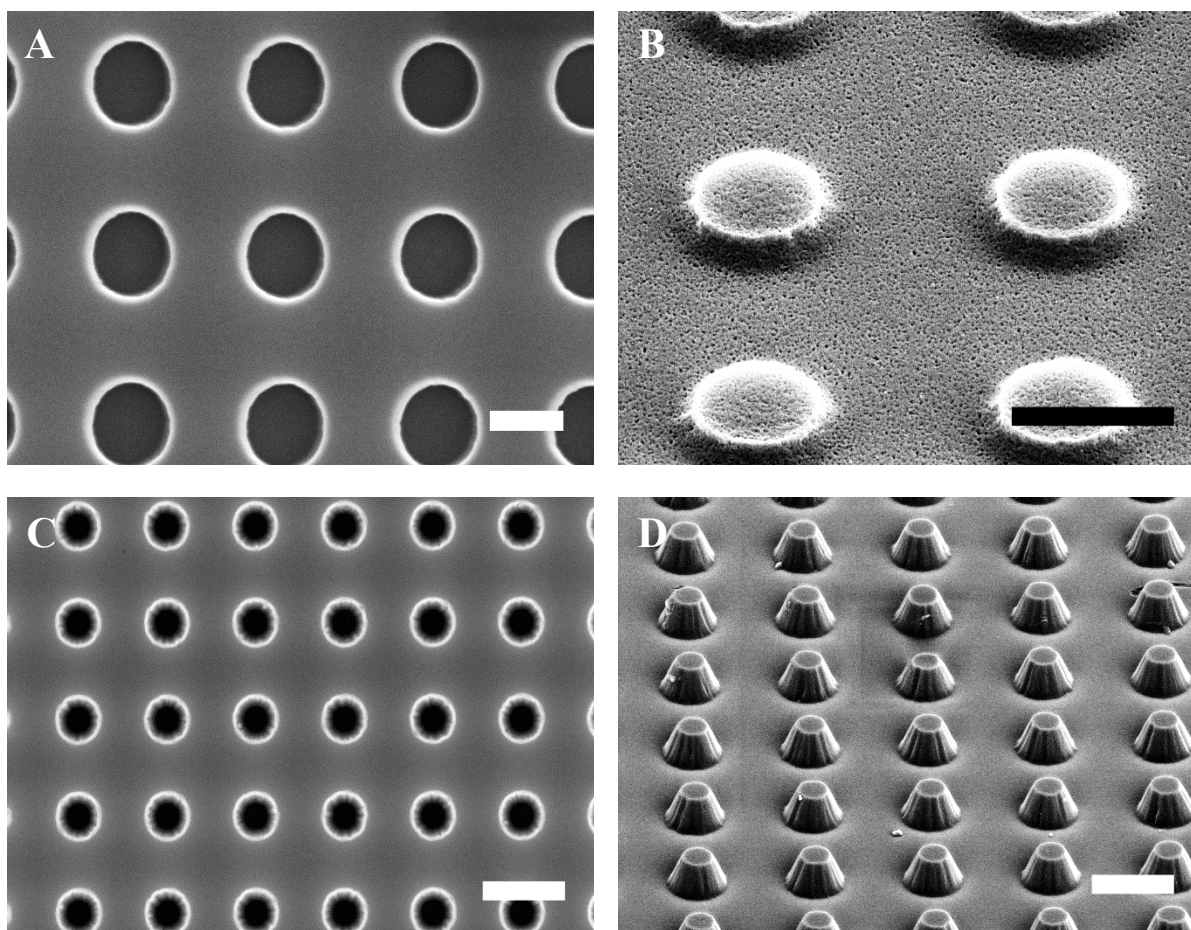
Figure 2.4. SEM images of silica molds and OrmoComp replicas. *A) A0.5 mold (D = 0.5 µm, P = 1 µm). Scale bar: 500 nm. B) A0.5 polymer replica with nanopillars of 100 nm in height. Scale bar: 500 nm. C) B0.75 mold (D = 0.75 µm, P = 1.5 µm). Scale bar: 1 µm. D) B0.75 polymer replica with nanopillars of 400 nm in height. Scale bar: 1 µm.*

The simplest structural element of all the arrays can be described as a conical frustum. In geometry, a conical frustum is a portion of a cone created by slicing the top off a cone (Figure 2.5.). All arrays were 1 x 1 cm in size, with labels and dash lines around the topography. The depth of the nanostructures was characterized using a Dektak profilometer (3030 Sloan/Veeco).
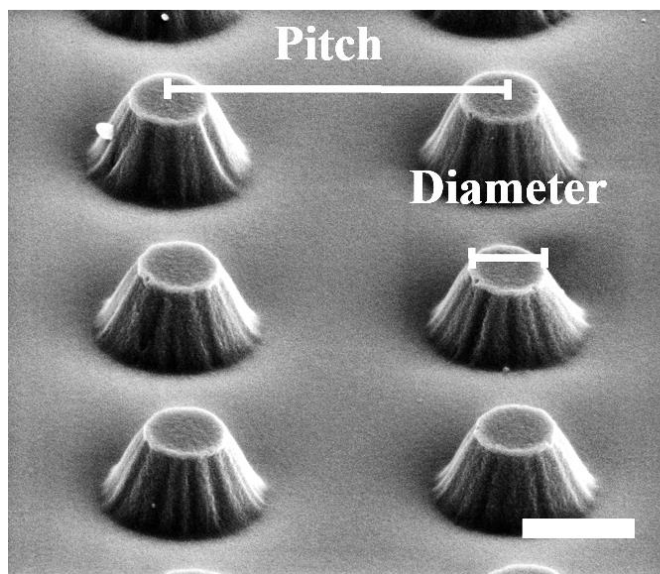
Figure 2.5. SEM image of polymer nanopillars. *Nanopillars replicated in the OrmoComp polymer are frustum shaped with a 740 nm base and 335 nm top diameter (substrate B0.75). Scale bar: 500 nm.*

A total of eight topographies with different diameters (0.5 µm, 0.75 µm, 1 µm, 2 µm) and heights (0.1 µm and 0.4 µm) were used in this thesis (Table 2.1.). The pitch of all the arrays was twice their respective diameter (1 µm, 1.5 µm, 2 µm, 4 µm).

Table 2.1. Dimensions of the topographies used in the presented thesis.

Substrate	Diameter (µm)	Pitch (µm)	Height (µm)
A0.5	0.5	1	0.1
A0.75	0.75	1.5	0.1
A1	1	2	0.1
A2	2	4	0.1
B0.5	0.5	1	0.4
B0.75	0.75	1.5	0.4
B1	1	2	0.4
B2	2	4	0.4

2.1.5. Surface modification

The received replica wafers were cut using a diamond cutter. Substrates were embedded on 35 mm dishes with a hole punched in the bottom. The outside edge of the hole was coated with a small amount of polydimethylsiloxane (PDMS, Sylgard 184 Silicone Elastomer Kit) and the hole was covered by the substrate (Figure 2.6.). PDMS was cured for 3 h at 85°C. Dishes were sterilized by briefly dipping them in 70% ethanol and dried with N_2 gas. Substrates were coated with 3 ml per 35 mm well of 1% poly-L-lysine (Sigma-Aldrich; 16.67µg/ml in sterile H_2O) in HBSS for 1 h at room temperature. Wells were washed once with an equal volume of HBSS and stored at 4°C.
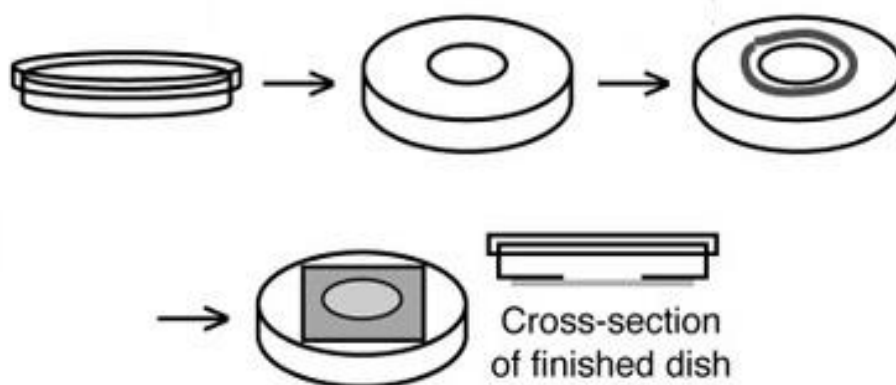
Figure 2.6. A schematic representation of substrate embedding. *A 35 mm dish is punched on the bottom side to create a hole (1 cm diameter). The outside edge of the hole is coated with PDMS and the hole is covered with a substrate.*

2.2. **Plasmid preparation**

2.2.1. **Transformation of competent cells**

The initial sample of p^{CMV}–Lifeact–TagRFP cDNA plasmid was obtained from Ibidi (Figure 2.7.). One Shot TOP10 chemically competent *E. coli* cells (Life Technologies) were transformed with the plasmid. Briefly, 50 µL of competent cells were thawed on ice and 1 µL of plasmid was added. The cells were incubated on ice for 5 min, heat-shocked for exactly 30 sec at 42ºC followed by another 2 min incubation on ice. 250 µL of S.O.C. medium (20 g/L tryptone, 5 g/L yeast extract, 4.8 g/L MgSO4, 3.603 g/L dextrose, 0.5g/L NaCl, 0.186 g/L KCl; Life Technologies) was aseptically added to help cell recovery. The cells were then placed in a shaking incubator for 1 h (37ºC, 200 rpm) and spread on a preheated kanamycin selective LB agar plate (10g/L tryptone, 5 g/L yeast extract, 5 g/L NaCl, 50 µg/mL kanamycine; Sigma-Aldrich). The plates were incubated overnight at 37°C.

Figure 2.7. Schematic representation of p^{CMV}–Lifeact–TagRFP cDNA plasmid. *The Lifeact sequence codes for a 17-amino acid actin-binding peptide. This sequence is fused to a fluorescent marker (TagRFP). The vector backbone contains immediate early promoter of cytomegalovirus (P^{CMV}) for protein expression and SV40 polyadenylation signals (SV40 poly A) for proper processing of the 3'-end of the reporter mRNA. SV40 early promoter (P^{SV40}) provides neomycin and kanamycin resistance genes (KanR/NeoR). KanR is used for selection of transformed E. coli while NeoR is used to select stably transfected eukaryotic cell using kanamycin and neomycin, respectively. Additionally, it contains ColE ori for plasmid replication in E. coli and f1 ori for producing ssDNA.*

2.2.2. Plasmid purification

A single colony from a freshly streaked kanamycin selective plate was picked and a starter culture of 5 ml LB medium containing 50 µg/ml of kanamycin was inoculated. The starter culture was incubated overnight at 37°C with shaking (200 rpm) and diluted 1/1000 into kanamycin selective LB medium (1 L). The culture was grown overnight at 37°C with shaking (200 rpm). Plasmid DNA was purified from transformed *E. coli* cells using the Qiagen Plasmid Maxi Kit and the provided protocol. Bacterial cells were harvested by centrifugation at 5000 g for 15 min at 4°C and the pellet was resuspended in 10 ml of buffer P1 containing 100 µg/ml of RNase A and

LyseBlue reagent (1:1000). 10 ml of buffer P2 was added and thoroughly mixed by vigorously inverting the sealed tube 4–6 times until homogeneously colored blue suspension was achieved. The suspension was incubated at RT for 5 min. 10 ml of chilled buffer P3 was added, and the tube vigorously inverted 4–6 times until the suspension became colorless with precipitated material containing genomic DNA, proteins, and cell debris. The suspension was incubated on ice for 20 min. The lysate was cleared of precipitated material using QIAfilter Cartridges. QIAGEN-tip 500 column was equilibrated with 10 ml of buffer QBT and the lysate was loaded. After the column emptied, it was washed twice with 30 ml of buffer QC to remove contaminants. DNA was eluted with 15 ml of buffer QF followed by precipitation with 35 ml of isopropanol (4°C) and centrifugation at 5000 g for 30 min at 4°C. The supernatant was carefully decanted and the DNA pellet washed with 2 ml of 70% ethanol to remove precipitated salts and replace isopropanol, followed by centrifugation at 5000 g for 10 min. The supernatant was carefully decanted without disturbing the pellet which was then air-dried for 20 min. DNA was dissolved in Milli-Q water and its concentration determined using a spectrophotometer by measuring the absorbance at 260 nm (DNA). The purity was determined by measuring the absorbance at 280 nm (aromatic amino acids) and calculating the A_{260}/A_{280} ratio (1.7-2.0). The plasmid concentration obtained was 0.85 µg/µl. The sequence of the plasmid DNA was verified by sequencing in the Eurofins Genomics Facility (Ebersberg, Germany).

2.3. Primary cell culture

2.3.1. Dissection of embryonic cortex

Pregnant Wistar female rats were acquired from Charles River Wiga GmbH (Sulzfeld, Germany) and handled by a certified technician. For all cell culture experiments in this thesis cortical neurons from rat embryos at day 18 of gestation (E18) of either sex were used (Figure 2.8.A). Briefly, pregnant females were anesthetized by carbon dioxide inhalation and decapitated. Following decapitation, embryos were removed from the uterus and stored briefly on ice. Embryos were removed from the amniotic sac and decapitated. The heads were transferred in cold calcium- and magnesium-free Hank's Balanced Salt Solution (HBSS, Sigma-Aldrich) supplemented with 20 mM glucose (Sigma-Aldrich), 1 mM sodium bicarbonate (NaHCO$_3$, Sigma-Aldrich), 1 mM sodium pyruvate (C$_3$H$_3$NaO$_3$, Sigma-Aldrich) and 10 mM HEPES (Sigma-Aldrich), and washed

twice by gently tilting the dish for 5-10 sec to remove all traces of blood. A stereomicroscope and curved forceps were used to extract the rat embryo's brain by pulling off the skin and skull and placing the brain in a separate dish with cold supplemented HBSS (Figure 2.8.B). The hemispheres were separated and cerebral cortices isolated by removing the midbrain and meninges (Figure 2.8.C). Dissected cortices were collected in a clear conical tube with cold Hibernate A medium (Life Technologies) used for long term preservation of viable embryonic brain tissue and stored at 4ºC.

2.3.2. Dissociation and transfection of primary cortical neurons

Cortices were either used immediately or 3 days after dissection. Cortical tissue was dissociated by trypsinization using 0.05% trypsin/ethylenediaminetetraacetic acid (EDTA, Life Technologies) for 15 min at 37ºC. The tissue was washed twice with Neurobasal medium (Life Technologies) supplemented with 1% (vol/vol) B-27 (Invitrogen), GlutaMAX (0.5 mM, Invitrogen) and gentamycin antibiotic (50 µg/ml) followed by gentle mechanical trituration with a 1 ml micropipette. The suspended cells were rested for 3 min to allow cell aggregates and glial cells to settle on the bottom of the tube. The upper 2/3 of the suspension were transferred to a new tube, centrifuged at 200 g at RT for 3 min, and the supernatant was carefully removed. Transfection was done using the Amaxa Rat Neuron Nucleofector Kit (Lonza). The neuronal pellet was resuspended in 200 µl of Nucleofector transfection solution (Lonza) and transferred into an Amaxa cuvette (Lonza) loaded with 12 µg of Lifeact-RFP cDNA plasmid. The cells were electroporated using the Amaxa Nucleofector device (Lonza), program G-013. Immediately after electroporation, 1 ml of preheated RPMI 1640 medium (Roswell Park Memorial Institute, Life Technologies) supplemented with 1% (vol/vol) Fetal Bovine Serum (Sigma-Aldrich) and 0.5 mM L-Glutamine (Invitrogen), was added to the cuvette to promote recovery and resealing of the cell membrane. Live cells were counted using a trypan blue exclusion assay. Briefly, 40 µl of RPMI and 20 µl of cell suspension was added to 20 µl of trypan blue solution. The mix was introduced into a Neubauer chamber (10 µl) and the live cells (white) were counted (Figure 2.8.D). The cell concentration was calculated using the formula:

$$Concentration\ (cell\ /\ mL) = \frac{Number\ of\ cells * 10\,000}{Number\ of\ squares * Dilution}$$

Cells were diluted in supplemented RPMI medium, and seeded on substrates at a density of 50 000 cells/ml. After settling at RT for 10 min, cultures were transferred to an incubator (5% CO_2, 37ºC, 100% humidity), and RPMI medium was changed after two hours with warm supplemented Neurobasal medium to remove cells that did not adhere to the surface.

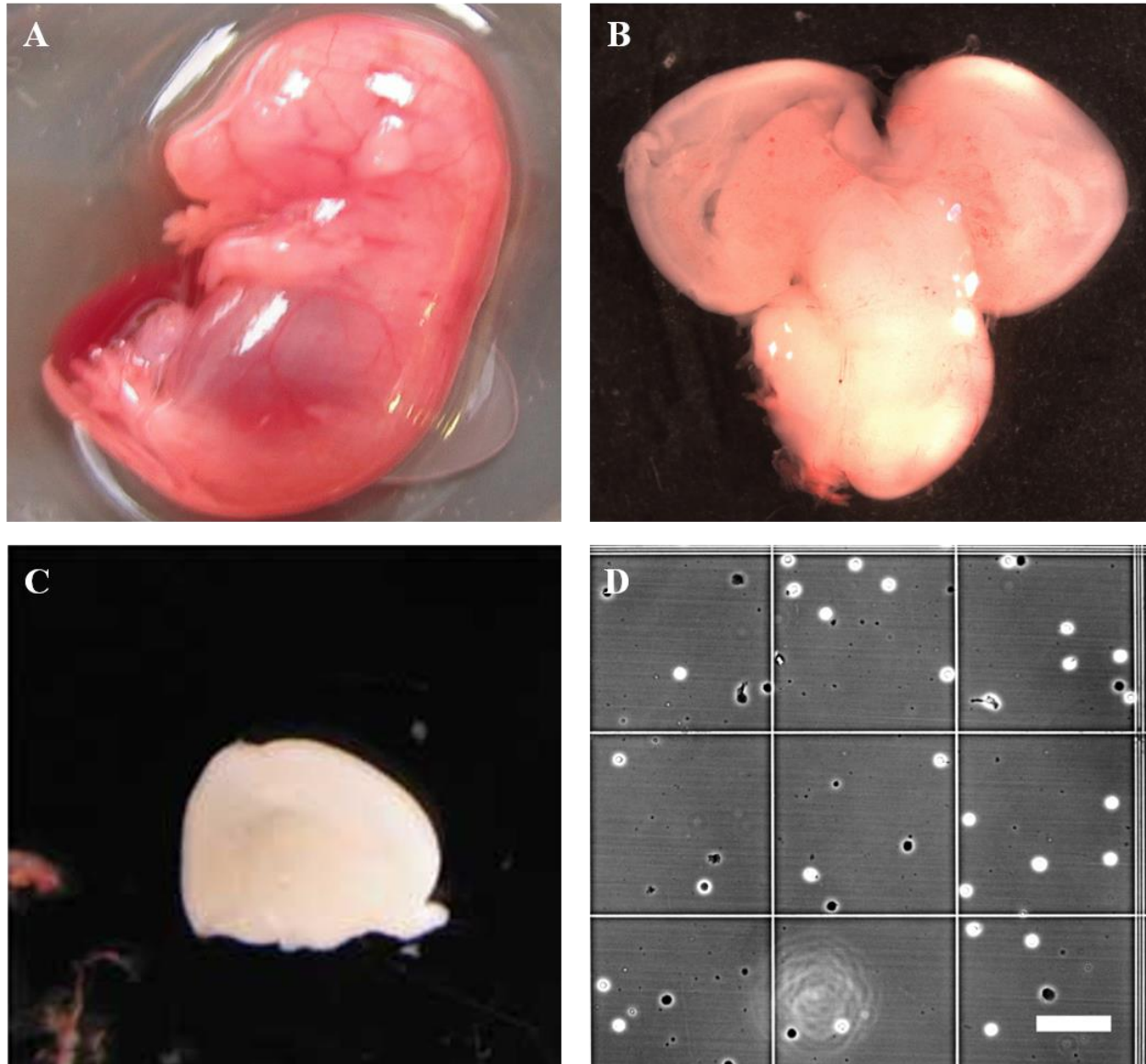*Figure 2.8.* *Rat embryo at day 18 of gestation (**A**) is decapitated and its brain is dissected (**B**). Cerebral cortices are isolated (**C**) and the tissue is dissociated. Dissociated cells are counted post-transfection using a trypan blue assay. Disrupted membranes of dead cells are permeable to trypan blue while live cells have non-permeable membranes (white) (**D**). Scale bar: 100 μm.*

2.4. Time-lapse microscopy

Time-lapse microscopy (live cell imaging) was used to study the influence of structural confinements on cellular development. Live cell imaging provides conditions that support cell development and the ability to observe it in real time. Time-lapse images were acquired every 30 min for 3 days starting from 5 h after plating. Experiments were performed using an Axio Observer.Z1 (Zeiss) inverted microscope equipped with an incubation chamber (PeCon) with a temperature, CO_2, and humidity control. Additionally, the setup was equipped with a Colibri fluorescence system (Zeiss), a PCO.edge 5.5 scientific complementary metal-oxide-semiconductor (sCMOS) camera, a motorized xy-table (Merzhäuser) and a Definite Focus Unit (Zeiss), which is used to stabilize the focus over time. The system is capable of long-term imaging of multiple positions maintaining *in vitro* culture conditions with a temperature of 37ºC, 5% CO_2, and 100% humidity and is controlled with ZEN 2012 software (Zeiss). All images were acquired using a 40x air objective (LD Plan-Neofluar, 0.6 NA, Ph2, Zeiss).

The light intensity was chosen as low as possible to reduce phototoxicity but at the same time ensuring good image quality. The exposure time for the fluorescence image was 400 ms at 35% light intensity of the 570 nm LED while the bright field image was acquired with an exposure time of 50 ms with a light source at 3.2 V. To receive detailed information about the dynamics of neuronal growth and actin cytoskeleton a high resolution was chosen with an image size of 2560 pixel $\times$ 2160 pixels resulting in a frame of 416 µm $\times$ 315 µm (pixel size: 0.163 µm $\times$ 0.163 µm).

Time-lapse sequences were processed using Fiji software. Briefly, the sequences were stabilized to correct for sample drift in the xy-plane during imaging using Fiji's StackReg plugin. The axon growth was traced manually using the MTrackJ plugin whereby only the longest neurite or branch was measured. More than 40 cells from at least 2 independent culture dishes for each substrate were analyzed and the data was processed using R package.

2.5. Fluorescent immunocytochemistry

Neuronal cell morphology and individual cell components such as axons and dendrites were visualized using fluorescent immunocytochemistry. After three days of live cell imaging (3 DIV),

the cells were rinsed three times with preheated phosphate buffered saline (PBS) prior to fixation for 15 min at RT with 4% paraformaldehyde diluted in PBS. Subsequently, the substrates were rinsed three times with PBS and permeabilized with 0.3% Triton X-100 (Sigma-Aldrich) in blocking buffer (BB, 2% bovine serum albumin and 2% heat inactivated goat serum diluted in PBS, Sigma-Aldrich) for 13 min at RT followed by another three rinsing steps with PBS. Unspecific binding sites were blocked with BB at 4ºC in the dark overnight. Afterwards, substrates were rinsed three times with PBS and incubated with primary antibodies. Antibodies against β-III-tubulin (2 µg/ml, rabbit, abcam) and Tau-1 (2 µg/ml, mouse, Sigma-Aldrich) were diluted in BB 1:500 and 1:300 respectively. A drop of 150 µl of the antibody solution was deposited on a plastic sheet covered with parafilm for every substrate and the substrates were placed cells down on the droplet. The primary antibody was incubated for 2.5 h at RT in a wet and dark chamber. Subsequently, the substrates were thoroughly rinsed three times with PBS before they were incubated with the secondary antibody. The secondary antibodies used were goat anti-mouse Alexa Fluor 633 and goat anti-rabbit Alexa Fluor 488 both diluted to 1:500 in BB. A drop of 150 µl BB with secondary antibodies, and 4',6-Diamidin-2-phenylindol (DAPI, 1:1000) was deposited on a parafilm covered plastic sheet and the substrates were incubated for 2 h at RT in a dark wet chamber. Finally, the incubated substrates were rinsed three times with PBS and twice with Milli-Q water before being embedded in fluorescent mounting media (Dako) and dried overnight.

Fluorescence microscopy was performed using an Axio Imager Z1 microscope (Carl Zeiss) equipped with an Illuminator HXP120 light source and a digital AxioCam MR R3 CCD camera. Images were taken with a 20x objective and analyzed using Fiji software to obtain cell viability, neurite length (NeuronJ), neurite number, axonal initiation and path finding angles, and soma area. Neurons that formed clusters were not included in analysis. Fluorescent images were oriented with the grid of structures aligned to vertical and horizontal and all angles measured with respect to the direction of the pattern. The initiation angle was measured before the first change in direction of the axon and the last angle of the axon was measured as the path finding angle (Figure 3.4.C). The axon turns between initiation and final path finding angles were not considered. Cortical neurons were characterized with antibodies against β-III-tubulin, which is specifically expressed in neurons of the central and peripheral nervous system (Roskams et al. 1998). Anti-tau-1 antibodies were used to visualize axons since Tau-1 is a microtubule-associated protein expressed in axons of

cortical neurons (Lei et al. 2010). More than 200 cells from at least 3 independent culture dishes for each substrate were analyzed and the data processed using R package.

2.6. Statistical analysis

Data was analyzed using R package. Quantitative measurements were analyzed via a Kolmogorov-Smirnov test to assess normality and then compared using the nonparametric Mann-Whitney U test. Multiple comparisons correction was done using the Holm-Bonferroni method. All boxplots are Tukey type with the median denoted as a red line and the mean as a black dot. A p-value less than 0.05 was considered significant.

3. RESULTS

Primary cortical neurons were cultured on OrmoComp polymer nano- and micropillar substrates to investigate the influence of different topographical features on neuronal development. General morphological features including axonal and dendritic length, neurite number, soma area, and axon guidance of cortical neurons cultured on nanostructured substrates were analyzed after 3 DIV, when neurons have already defined axons and dendrites. Neurons growing on nanostructured substrates were compared to those on flat polymer surfaces. Axon guidance was evaluated by measuring the initiation and final pathfinding angle of the axon. All fluorescent images were oriented with the grid of structures aligned to the vertical and horizontal axes. Additionally, time-lapse imaging was used to investigate the dynamics of neuronal development on different topographies including growth speed, directionality, mean squared displacement and the angle distribution of the growing axon.

3.1. Viability of cortical neurons on OrmoComp substrates

Cortical neurons were isolated from E18 rat embryos and cultured on substrates with different nanopillar dimensions and spacings and compared to control cultures on PLL-coated glass coverslips. Cells were electroporated to introduce Lifeact-RFP plasmid in order to visualize the actin cytoskeleton. The viability of control samples was taken as 100% and the viability of all other substrates was normalized to the control samples. The viability of both transfected and non-transfected cortical neurons was assessed using fluorescent immunocytochemistry and compared to their respective glass coverslip controls. A cortical neuronal cell was considered viable if it was positive for β-III-tubulin staining. Both flat and nanostructured polymer substrates supported neuronal growth with a relative viability (viability compared to controls on glass coverslips) of 97.2% ± 6.34% and 96.53% ± 3.26% for non-transfected neurons after 3 DIV, respectively. Transfected neurons had a lower relative viability of 79.1% ± 7.59 % on the flat polymer substrate and 68.1% ± 11.15% on nanostructured substrates (Figure 3.1.) The absolute viability of transfected neurons after 3 DIV on glass coverslips was 9.32% ± 1.1%. Absolute viability was defined as the ratio of the number of live cells and the total number of cells.
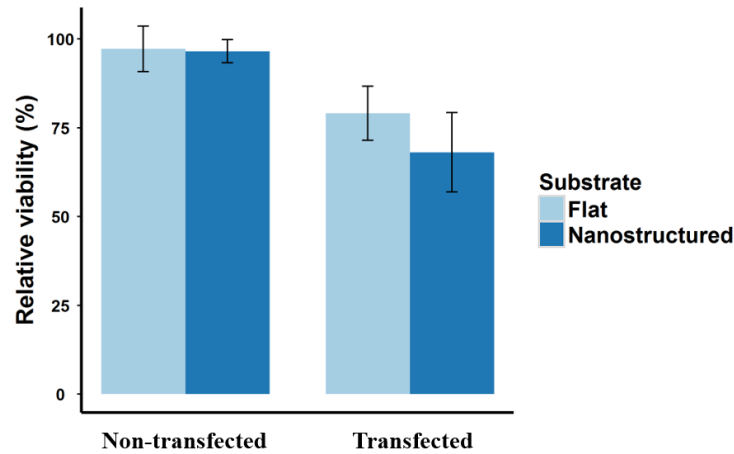
Figure 3.1. Relative viability of non-transfected and transfected cortical neurons on OrmoComp polymer substrates. *The viability of transfected and non-transfected cells was normalized to the viability on glass coverslip controls for each group. Data for each group was measured from at least 5 independent cultures and is presented as mean ± SEM.*

3.2. Neuronal morphology on 100 nm high nanopillars

In order to determine whether pillars of different diameters and pitches have an effect on neurite length and number, cortical neurons were fixed and stained with β-III-tubulin and Tau-1 markers after 3 DIV (Figure 3.2.). Analysis showed that all topographies with 100 nm high pillars promoted axon growth, resulting in longer axons compared to the flat polymer substrate (Figure 3.3.A). This effect was weaker for neurons growing on A2 pillars (2 µm diameter, 4 µm pitch) which had significantly shorter axons than those observed on other nanostructured substrates, although still longer than on flat polymer substrates. A similar effect was observed for dendritic lengths, with neurons cultured on A2 substrates having a similar distribution of dendrite lengths as on flat surfaces (Figure 3.3.B). The number of neurites per neuron was significantly reduced for A0.5, A0.75 and A2 substrates compared to flat substrates. Neurons cultured on A2 substrates had a significantly lower number of neurites than other nanostructured substrates (Figure 3.3.C). Neuronal adhesion to different surfaces was characterized by measuring the soma area after 3 DIV. Results show that neurons have a smaller soma area only on A2 (2 µm diameter, 4 µm pitch)

substrates compared to the flat substrate (Figure 3.3.D). Neurons cultured on A1 substrate had a significantly larger soma than both the flat substrate and the nanostructured substrates.
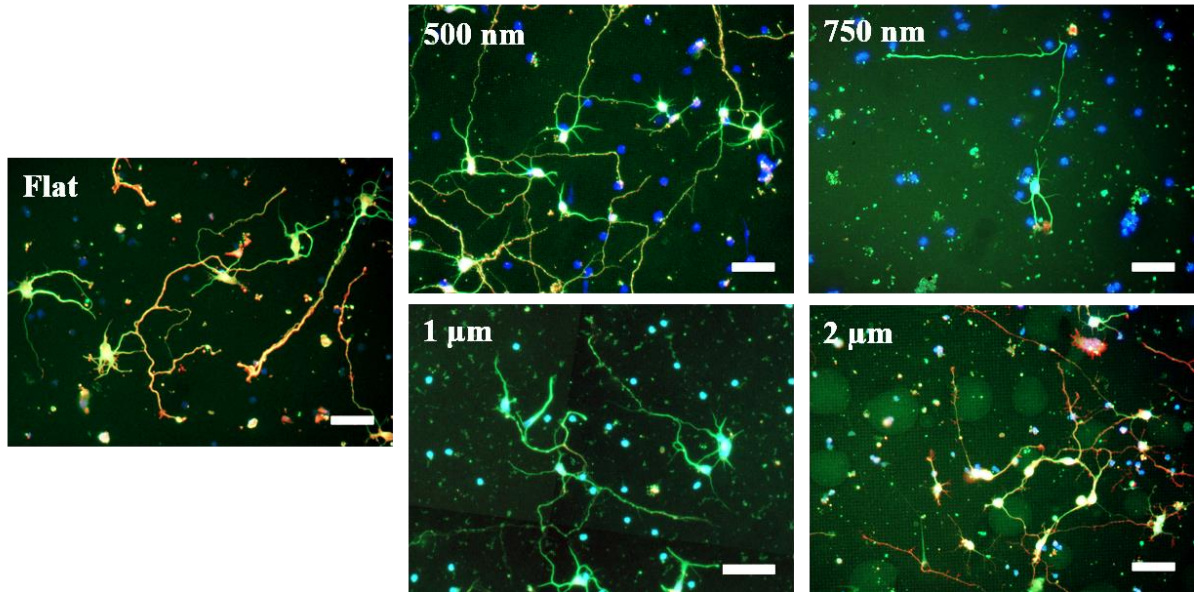

Figure 3.2. Cortical neurons on OrmoComp polymer substrate with 100 nm high pillars. *Neurons on nanostructured substrates had longer axons oriented along the pattern (here, vertically and horizontally oriented). Cells (3 DIV) were fixed and fluorescently labeled for: β-III-tubulin (green), Tau-1 (red), DAPI (blue). All substrates have a pitch twice as large as the diameter of their pillars. The frame title is the structure diameter. Scale bars: 50 μm.*
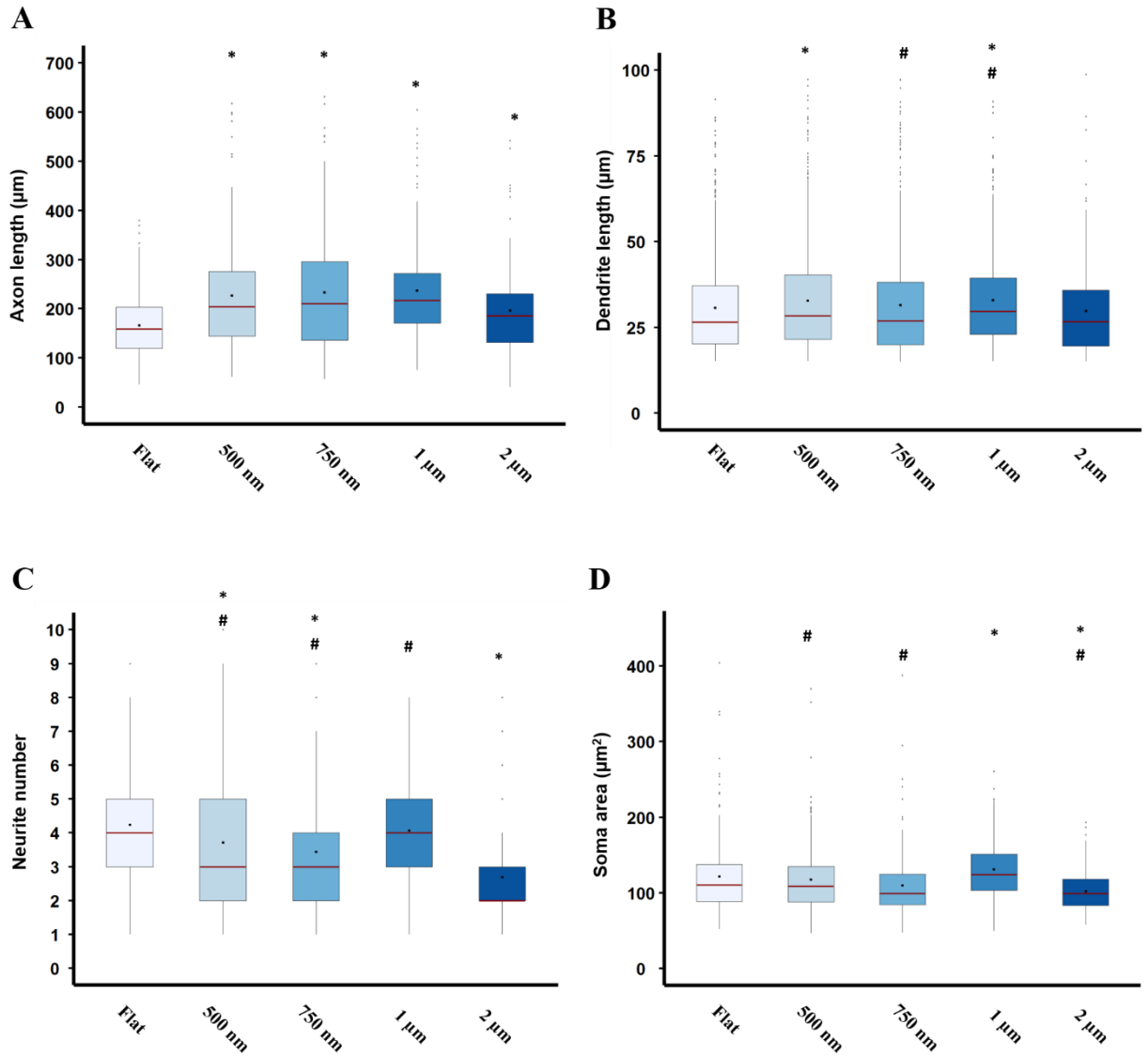
Figure 3.3. Effect of 100 nm high pillars on neuronal morphology after 3 DIV. A) *Axon lengths.*
B) *Dendritic lengths.* ***C)*** *Neurite numbers.* ***D)*** *Soma area. Legend: * indicates significant*
difference between flat polymer substrate and nanostructured substrates (0.05 significance level);
 # indicates significant difference between A2 substrate (B, C) or A1 substrate (D) and other
*nanostructured substrates (0.05 significance level).*

Since nanostructured polymer topographies have nanopillars uniformly ordered in the X and Y
directions, their effect on axon guidance was investigated. Axon initiation and final pathfinding
angles were measured and compared to those on flat substrates (Figure 3.4.A, B). Axons were

considered aligned to the pattern if the angles were 0º, 90º, or -90º relative to the direction of the pattern (Figure 3.4.C). Polar plots of the initiation and final pathfinding angles on flat substrates show a random distribution. On the other hand, axons extending on nanostructured substrates show a directional preference with the axon growing along the topographical features. Furthermore, the overall axon alignment to the pattern was determined as the ratio of the aligned axon length to the total axon length. Figure 3.4.D shows that topography has an influence on axon guidance with the highest alignment on the A0.5 (0.5 µm diameter, 1 µm pitch) and A0.75 substrates. Interestingly, pillars with a larger diameter (and pitch) showed a severe reduction in alignment, which approached that of the flat substrate for A2 pillars.
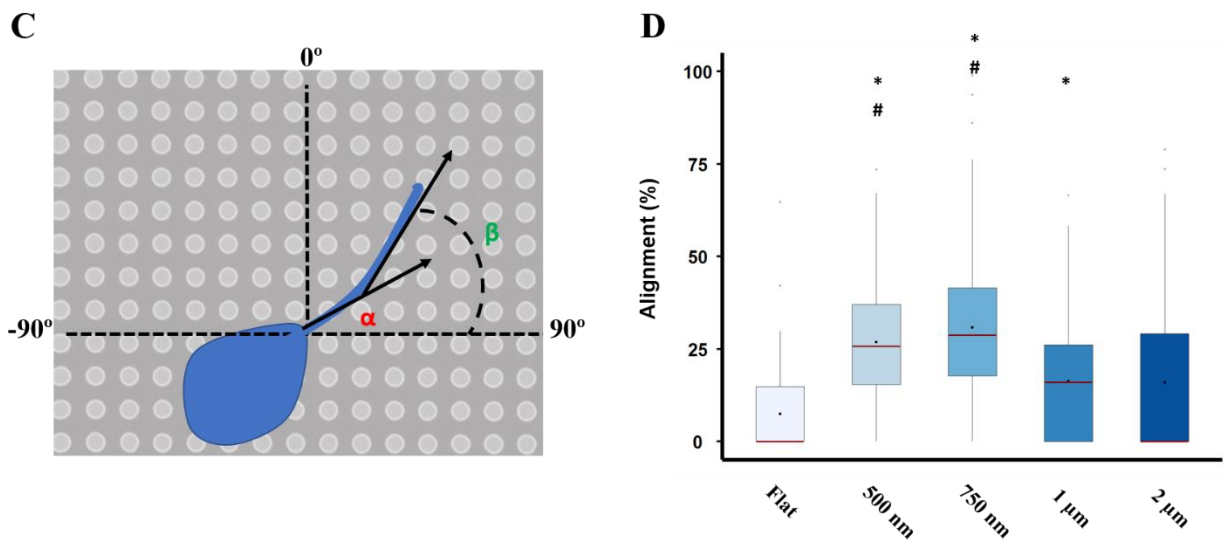
A
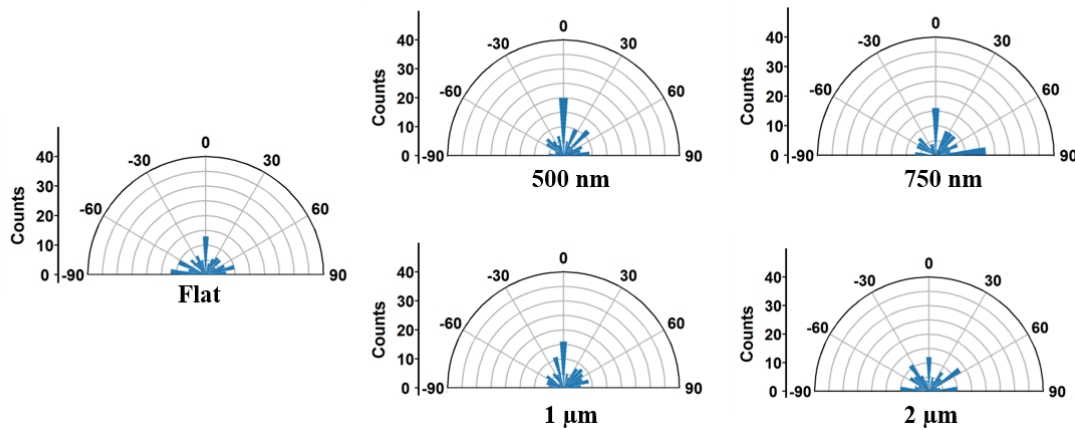
B
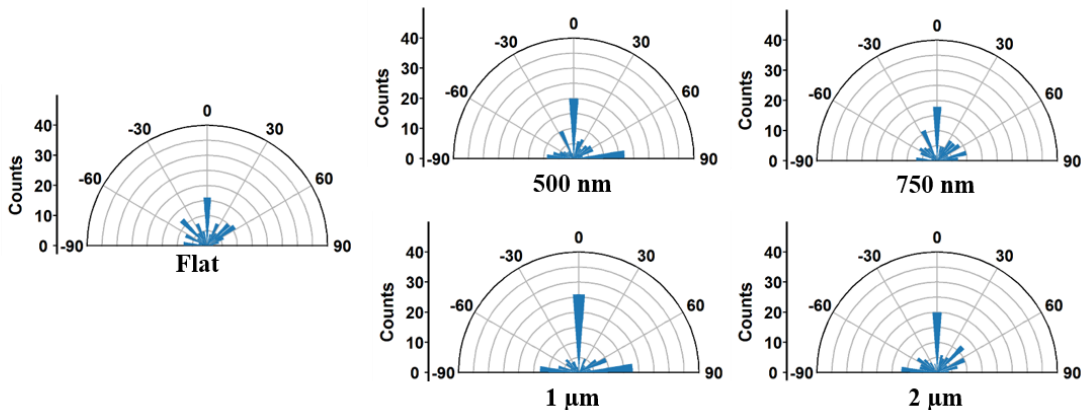
Figure 3.4. Effect of topography on axon guidance. A*) Distribution of axon initiation angles on flat and nanostructured substrates. **B) Distribution of axon final path finding angles on flat and nanostructured substrates. C) Schematics of initiation (α) and final path finding (β) angle measurements. D) Axon alignment to the pattern showing that the guidance effect diminishes on larger pillars (A1 and A2). A random direction was chosen for the flat substrate in measuring the axon alignment. Legend: * indicates significant difference between flat polymer substrate and nanostructured substrates (0.05 significance level); # indicates significant difference between A2 substrate and nanostructured substrates (0.05 significance level).*

3.3. Neuronal morphology on 400 nm high nanopillars

Cortical neurons were cultured on 400 nm high topographies with the same diameter and pitch as the 100 nm high topographies to determine the influence of pillar height on neuronal morphology and axon growth guidance (Figure 3.5.). All nanostructured topographies promoted axon growth with an increase in axon median length of ~100% in comparison to the flat substrate and ~50% compared to their corresponding 100 nm high counterparts (Figure 3.6.A). Such an increase was not present for the dendritic lengths, with only B0.5 (0.5 µm diameter, 1 µm pitch, 400 nm height) and B0.75 (0.75 µm diameter, 1.5 µm pitch, 400 nm height) exhibiting longer dendrites in comparison to flat surfaces (Figure 3.6.B). Neurons growing on nanostructured substrates had a lower number of neurites than those growing on flat and nanostructured substrates with 100 nm

height (Figure 3.6.C). Nanopillars with 400 nm in height reduced the soma area only for the B1 and B2 substrates (1 µm and 2 µm diameter, respectively, Figure 3.6.C) which is discussed in the following chapter.

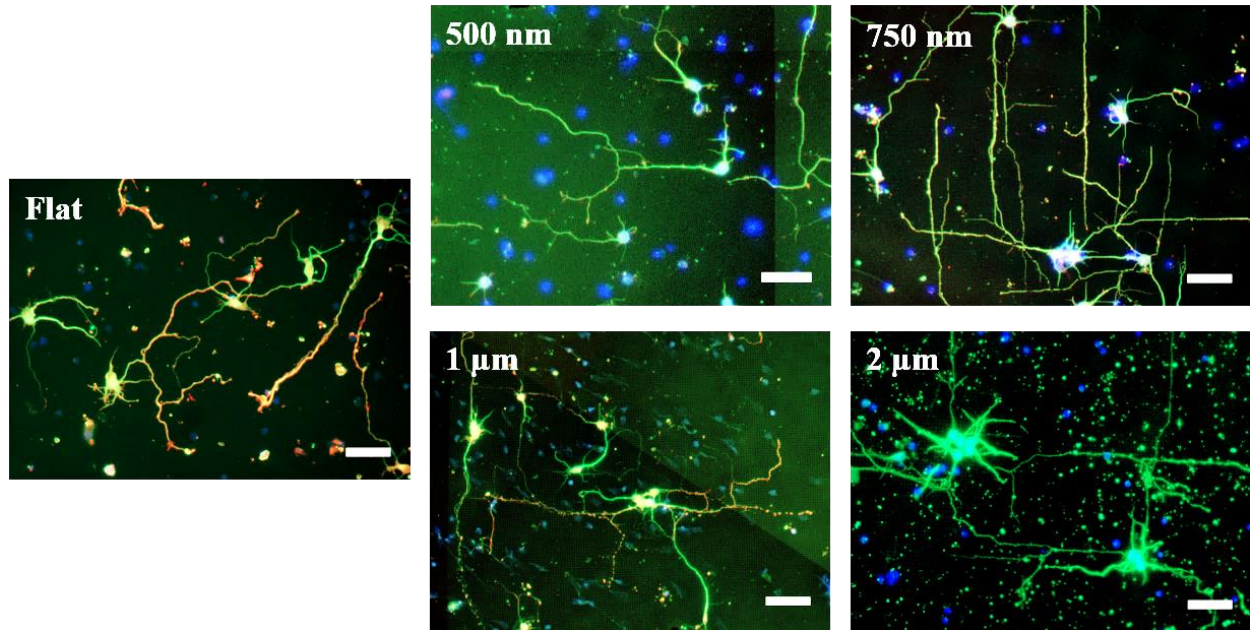*Figure 3.5. Cortical neurons on OrmoComp polymer substrates with 400 nm high pillars. All substrates show a strong axon guidance and growth promoting effect. Neurons (3 DIV) were fixed and fluorescently labeled for: β-III-tubulin (green), Tau-1 (red), DAPI (blue). All substrates have a pitch twice as large as the diameter of their pillars (diameter indicated in top left). Scale bars: 50 µm.*
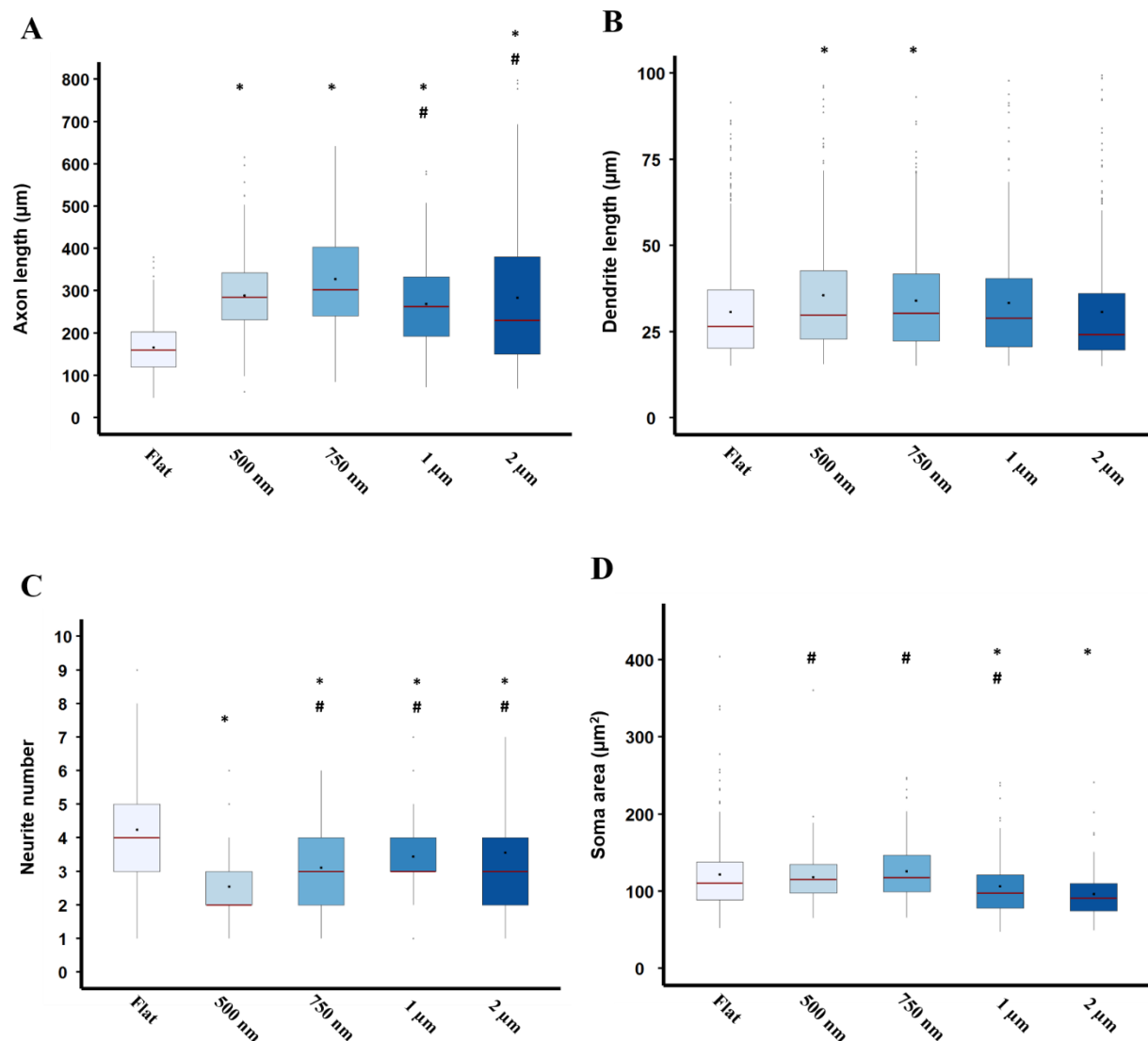
*Figure 3.6. Effect of 400 nm high topographies on neuronal morphology after 3 DIV. A) Axon lengths. B) Dendritic lengths. C) Neurite number. D) Soma area. Legend: * indicates significant difference between flat polymer substrate and nanostructured substrates (0.05 significance level); # indicates significant difference between B0.75 (A), B0.5 (C) or B2 (D) substrate and other nanostructured substrates (0.05 significance level).*

Pillars with 400 nm height had a strong effect on axon guidance with neurons having long axons growing in the direction of the pattern (Figure 3.5.). Axon initiation and pathfinding angles had a preferential distribution along the direction of the pillars (0º and ±90º, Figure 3.7.A, B) resulting

in a ~100% increase in axon alignment in comparison with the 100 nm substrates (Figure 3.7.C). B0.75 substrates exhibited the strongest guidance effect with axons being >50% aligned to the pattern.

C
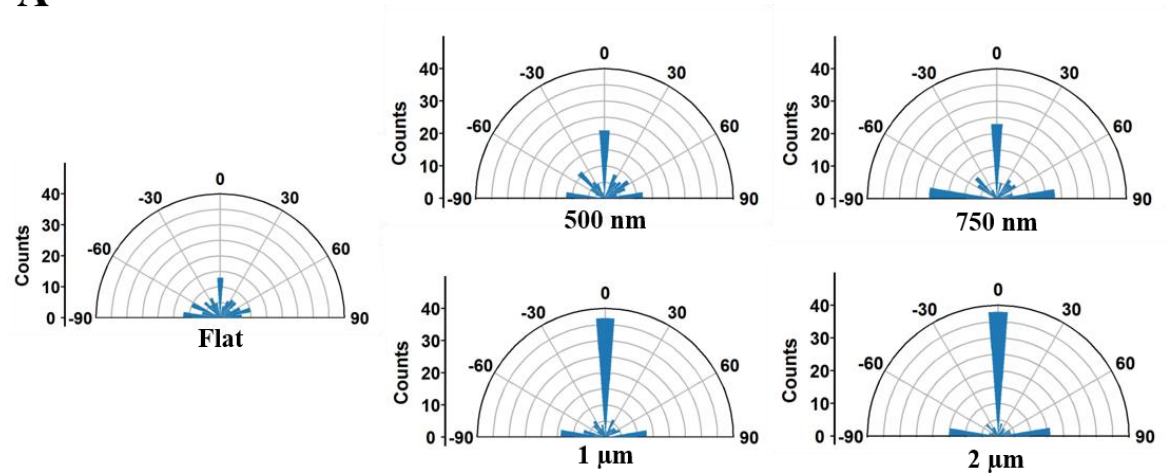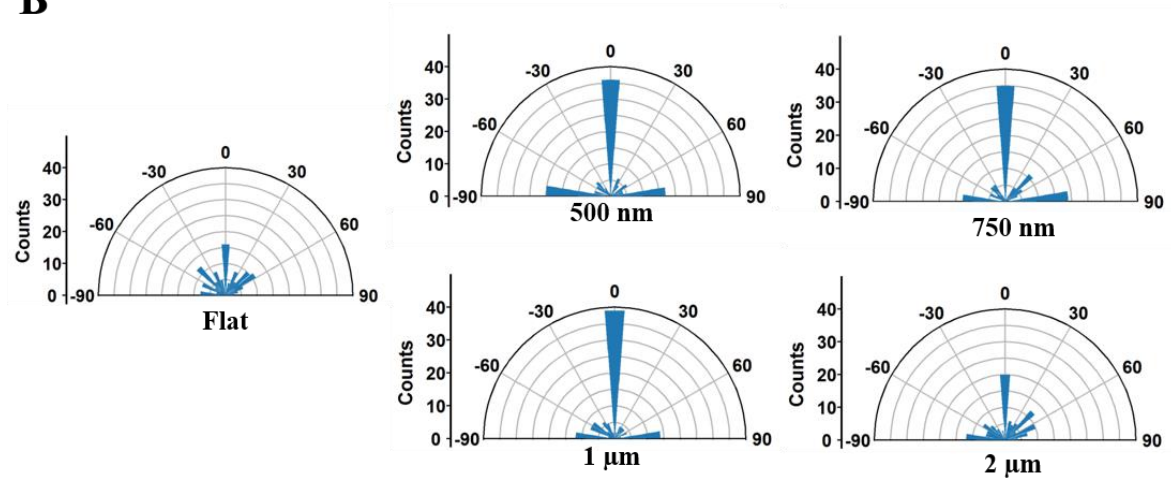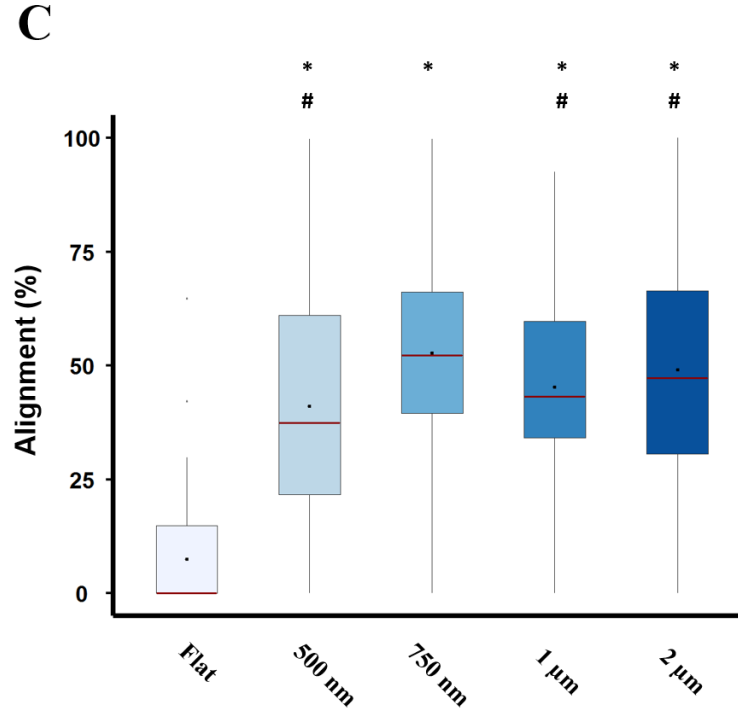
Figure 3.7. Effect of 400 nm high nanopillars on axon guidance. *A) Distribution of axon initiation angles on flat and 400 nm high nanostructured substrates.* ***B)*** *Distribution of axon final path finding angles on flat and 400 nm high nanostructured substrates.* ***C)*** *Axon alignment to the 400 nm high pattern. A random direction was chosen for the flat substrate in measuring the axon alignment. Legend: * indicates significant difference between flat polymer substrate and nanostructured substrates (0.05 significance level); # indicates significant difference between A0.75 substrate and nanostructured substrates (0.05 significance level).*

3.4. Time-lapse imaging of developing neurons

Time-lapse microscopy was used to investigate the dynamics of neuronal development on different topographies (Figure 3.10.E, F, G). Time-lapse images were taken in 30 min intervals for 3 days and the sequences were analyzed to obtain growth speed, directionality, mean square displacement, net displacement and the distribution of position vector angles of the growth cone relative to the pattern during axon elongation whereby only the longest neurite/branch was measured. The A2 and B2 substrates were not analyzed since no time-lapse sequences were obtained for these substrates. Growth cone speed was calculated as a ratio between the total distance traversed by the

growth cone and the total time. Directionality was calculated as a ratio of the net displacement and the sum of distances traveled by the growth cone between each time point (total distance). To evaluate the distance traversed by the growth cone in each time interval, MSD analysis was performed (Gorelik and Gautreau 2014). By obtaining the position vector of the cell trajectory at time t, mean squared displacement (MSD) is calculated using the following equation, in which brackets denote average over all times and for all N cells:

$$MSD(\Delta t) = \langle [x(t + t_0) - x(t_0)]^2 + [y(t + t_0) - y_0(t_0)]^2 \rangle_{t, N}$$

where $x(t_0)$, $y(t_0)$ is the growth cone position at starting time (t_0) and $x(t + t_0)$, $y(t + t_0)$ is the position at $t + t_0$. Nanostructured substrates increased the growth speed in comparison to the flat substrate with the exception of A0.5, which did not show a statistically significant increase in growth cone speed (Figure 3.8.A). However, pillars with the same dimensions but with a 400 nm height (B0.5 substrate) increased the growth cone speed. Figure 3.8.B shows that growth cones on 400 nm high pillars exhibit a higher directionality ratio meaning that axons extend more efficiently, i.e. larger MSD results in higher net growth. This effect was observed for the A0.75 substrate and all the 400 nm high substrates, where it was even more amplified. These results show that nanopillars, and especially 400 nm high nanopillars, promote axon growth speed and its directionality.
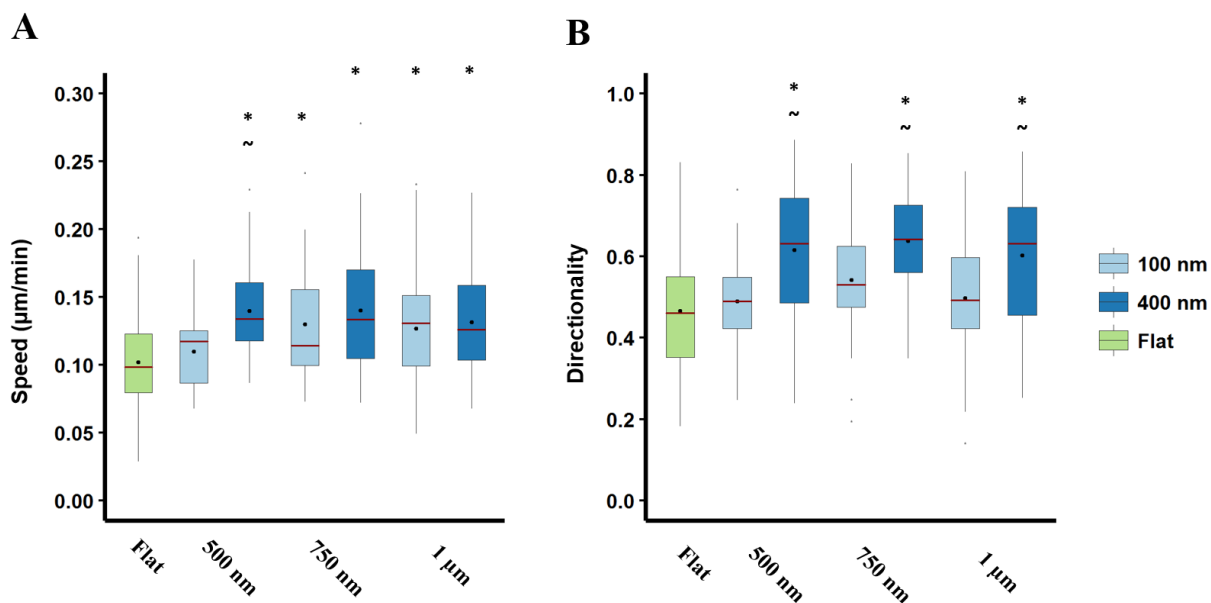
Figure 3.8. Effect of 100 nm and 400 nm high nanopillar polymer topographies on axon growth.
*A) An increase in growth cone speed was observed for neurons growing on nanostructured substrates. B) Neurons cultured on 400 nm high pillars exhibited more efficient growth (higher directionality ratio) compared to flat surfaces and surfaces with 100 nm high pillars. N > 40 cells from at least two independent cultures per substrate. Legend: * indicates significant difference between flat polymer substrate and nanostructured substrates (0.05 significance level); ~ indicates significant difference between 400 nm substrate and its corresponding 100 nm substrate (0.05 significance level).*

The mean squared displacement gives a measure of the area explored by the growth cone for any given time interval. The MSD analysis confirms that growth cones explored a larger area on nanostructured substrates (Figure 3.9.A, B). Importantly, the increased spatial exploration on nanostructured substrates was not only due to the increased growth cone speed (Figure 3.8.A), but also due to a more directional growth (Figure 3.8.B) resulting in a greater net displacement (Figure 3.9.C, D).
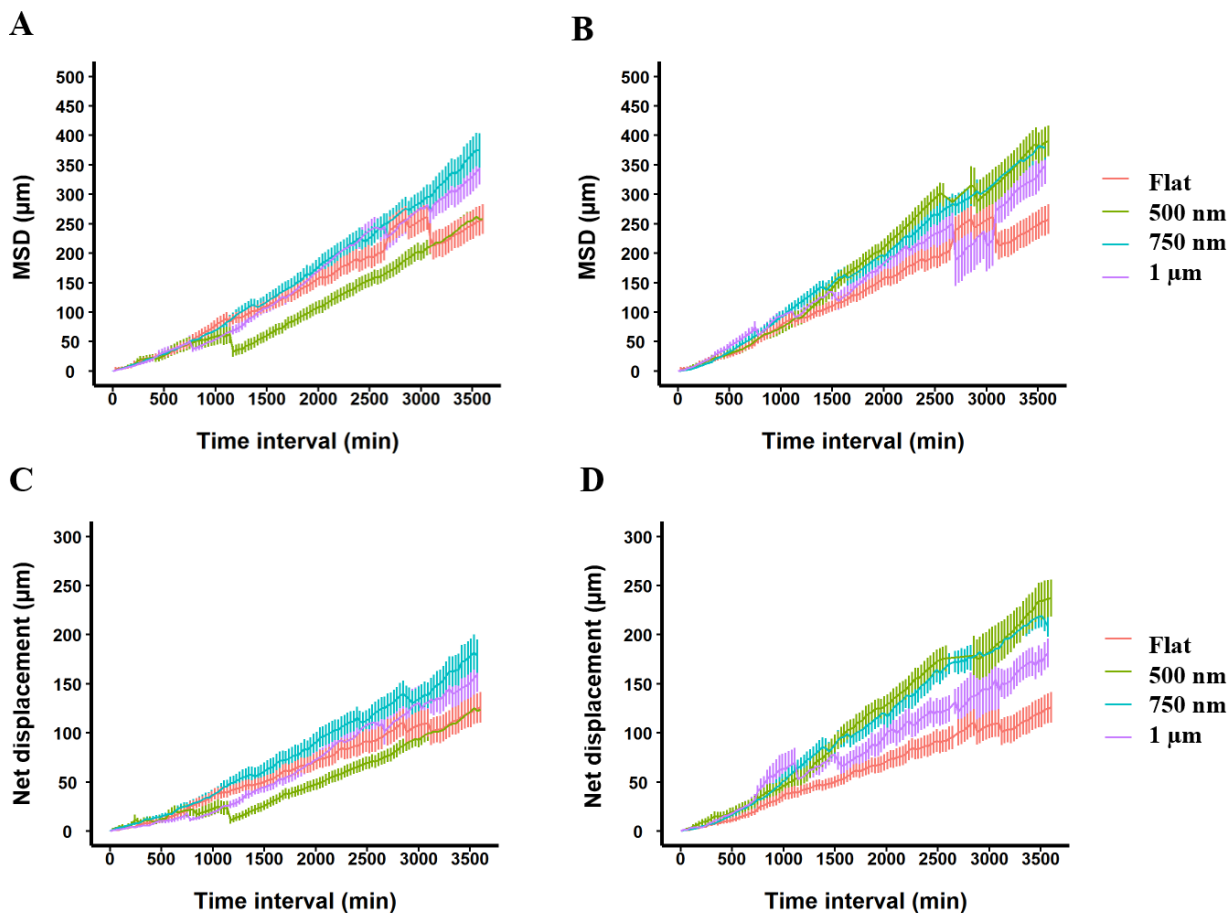
Figure 3.9. Dynamics of axon growth on 100 nm and 400 nm high nanopillar polymer topographies. *A) Mean squared displacement (MSD) for the 100 nm high substrates. **B)** Mean squared displacement for the 400 nm high substrates. **C)** Growth cone net displacement for the 100 nm high substrates. **D)** Growth cone net displacement for the 400 nm high substrates. MSD curves for the flat, A0.5 and B1 substrates have an apparent decrease in MSD values around 3000, 1100 and 2700 min, respectively. These are in fact experimental artefacts due to pausing and readjusting the focus during time-lapse imaging. N > 40 cells from at least two independent cultures per substrate.*

Figure 3.10. depicts distributions of displacement vector angles of the growth cone during axon elongation. These angles are defined as the angles of the in-plane component of the most recent displacement vector (going from the previous point to the current point) with respect to the x-y coordinate system of the image (with the origin taken at the previous point, Figure 3.10.A). The

polar plots show that these values are randomly distributed for flat substrates (Figure 3.10.B), while axons growing on nanostructured substrates tend to follow the pattern (Figure 3.10.C) with this preferential growth being even more pronounced on 400 nm high pillars (Figure 3.10.D).

Collectively, these findings indicate that the OrmoComp polymer substrates patterned with nano- and micropillars promote axon growth and guidance of cortical neurons with this effect being even more pronounced on higher pillars (Figure 3.10.E, F, G).
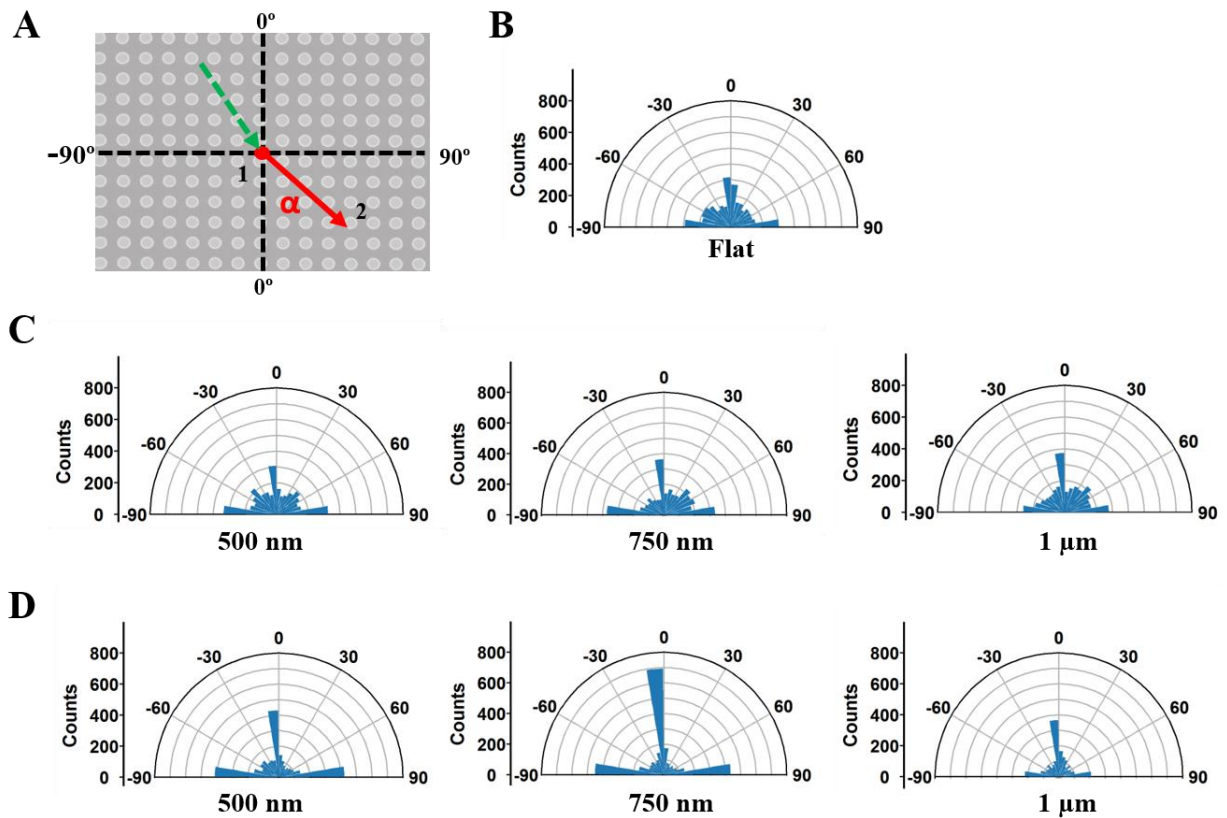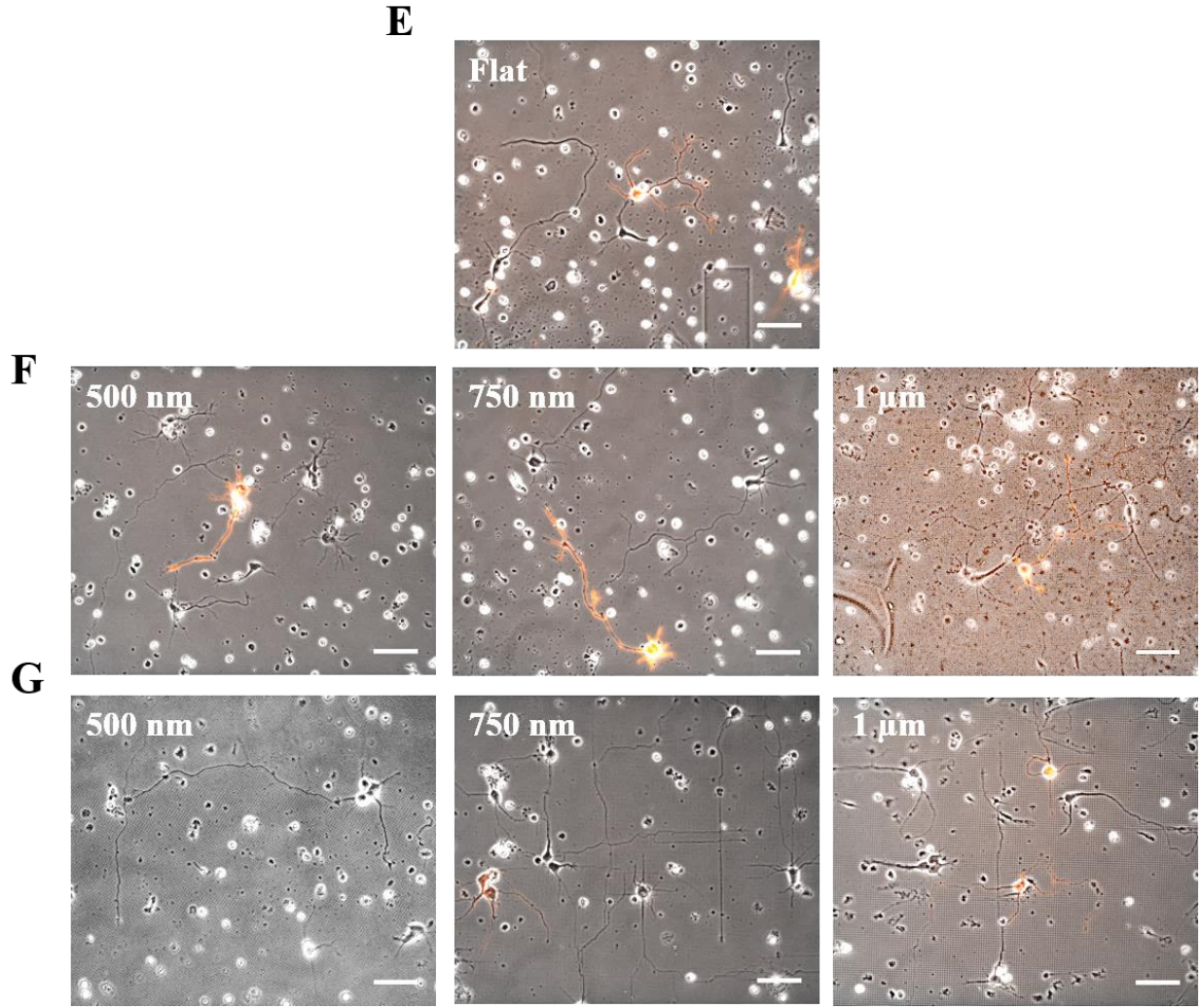
Figure 3.10. *A) Schematics of velocity vector angle measurements. Current angle (α) is defined by the vector going from the previous point (1) to the current point (2) and the xy-coordinate system of the image. **B)** Polar plot of the growth cone exploration angles on the flat substrate showing a random distribution of angles. **C)** Distribution of growth cone exploration angles on 100 nm high nanostructured substrates shows a preferential growth in the direction of the pattern. **D)** The preferential guiding effect is even stronger on 400 nm high nanostructured substrates. **E)** Neurons growing on flat polymer substrate. **F)** Neurons growing on 100 nm high nanostructured substrates. **G)** Neurons growing on 400 nm high nanostructured substrates. Some neurons in D, E, F are expressing a fluorescent actin marker (red). Scale bar: 50 µm.*

3.5. Transfection of primary cortical neurons

Cytoskeletal dynamics is considered to be key to how topography influences cell behavior, and several studies have demonstrated the importance of F-actin polymerization in response to topography (da Silva and Dotti 2002; Kang et al. 2014). Cortical neurons were transfected with Lifeact-RFP plasmid cDNA coding for an RFP-actin-binding peptide to investigate actin dynamics during the early stages of development. Electroporation of primary cortical neurons resulted in a 38.18% ± 5.51% survival rate as measured with the trypan blue exclusion assay immediately after transfection. Plasmid was successfully introduced with a transfection efficiency of ~20%, although cells had a low viability after 3 DIV (~10%). Neurons constitutively expressed the Lifeact-RFP peptide for more than 3 days (Figure 3.11.). Unfortunately, due to technical obstacles, time-lapse imaging of cytoskeletal dynamics could not be performed. The quartz wafers used in the fabrication of the substrate had a thickness of 0.545 mm preventing the use of high magnification objectives that could provide suitable resolution for the investigation of actin dynamics.
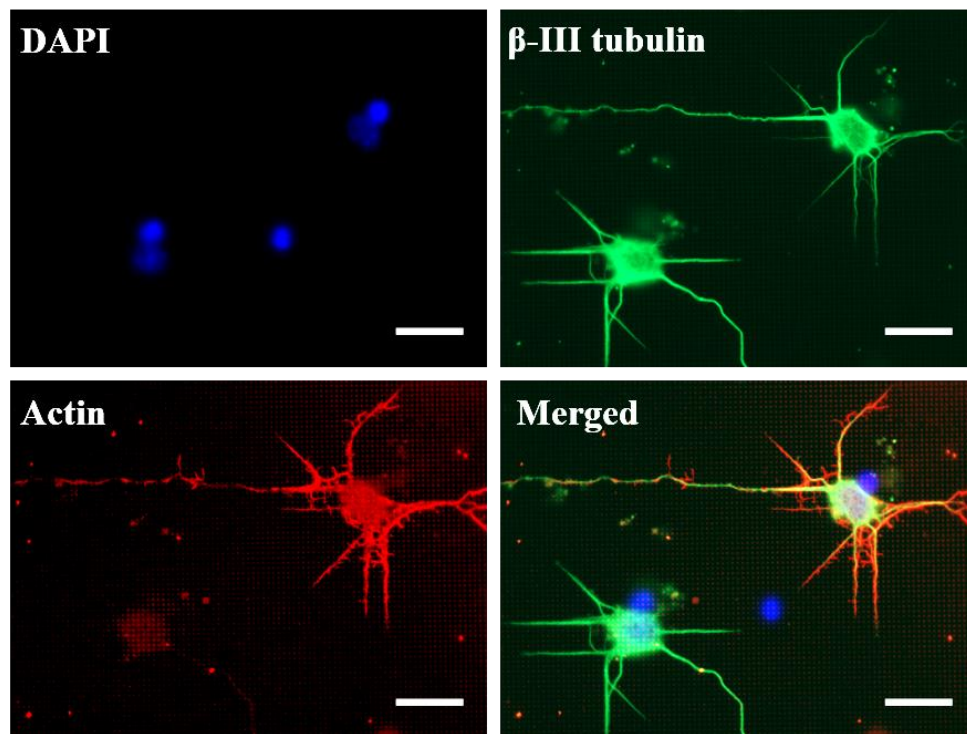

***Figure 3.11. Cortical neurons (3 DIV) expressing a fluorescent actin marker (red). β-III-*tubulin* (green), DAPI (blue). Scale bars: 10 μm.*

4. DISCUSSION

The architecture of the extracellular environment contains varying micro- and nanoscale features that influence complex cellular responses such as migration, proliferation, and differentiation. Although, interest in the influence of topographical cues on neuronal development started as an effort to more accurately model physical conditions *in vivo* for use in neuronal cultures (Rajnicek et al. 1997; Rajnicek and McCaig 1997), the field progressed to manipulation of neuronal development for applications in neural circuits, regenerative medicine, prostheses, etc. In the past two decades, a myriad of different materials has been used to investigate cell response to topographies ranging from microscale to nanoscale in recent years.

A total of eight topographies were used in this thesis to investigate the influence of topographical cues on the development and growth guidance of rat embryonic cortical neurons. The aim of this study was to investigate neuronal response to topographical features for possible applications in micro-electrode arrays and neural implants.

4.1. Viability of cortical neurons on OrmoComp polymer substrates

All substrates were fabricated from a polymer-ceramic hybrid material, OrmoComp, which was chosen because it is compatible with nanoimprint lithography and it has been proven biocompatible (Käpylä et al. 2014). Furthermore, the material was transparent, so neuronal development could be monitored with a microscope. In this study, neither flat nor nanostructured OrmoComp substrates had any detrimental effects on the viability of primary cortical neurons compared to controls on glass coverslips (Figure 3.1.). A significant decrease in relative viability of transfected neurons compared to non-transfected neurons cultured on PLL-coated glass coverslips was most likely due to the unreliability of the trypan blue exclusion assay. Embryonic cortical neurons were electroporated to introduce the Lifeact-RFP plasmid cDNA resulting in the disruption of the cell membrane. This meant that even if the cell was not dead it may be slightly stained with trypan blue. On the other hand, these cells could have been mortally wounded during dissociation or electroporation. Such cells were counted as live to avoid underestimation of the number of cells seeded. This could have led to plating more dead cells than intended resulting in an apparent decrease in viability of transfected cells measured after 3 DIV.

4.2. Neuronal development on 100 nm high nanopillars

In general, cells alter their morphology according to the topography of their surroundings. The most common morphological changes in neurons cultured on patterned substrates are increased neurite/axon length and alignment, decreased number of neurites, and faster development (Repić et al. 2016; Mahoney et al. 2005). Similar responses were observed in the presented thesis. Additionally, the response depends greatly on the topographical feature dimensions including diameter, height, and pitch. In this study, an increase in structure diameter and pitch reduced the aforementioned effects.

The first group of substrates consisted of pillars arranged in uniform rows and columns on the surface with a precisely defined diameter (500 nm, 750 nm, 1 µm, 2 µm) and interpillar pitch twice the size of the diameter (1 µm, 1.5 µm, 2 µm, 4 µm). This meant that the distance between the pillars was the same as their respective diameter. All topographies promoted neurite growth and this effect was stronger for the axons (Figure 3.3.A and B). This effect diminished on substrates with largest pillars (A2). While the length of neurites increased, their number decreased (Figure 3.3.C). Isotropic substrates have a guiding influence during axon growth (Spedden et al. 2014) and this effect was also observed in the present study, with both initial and final axon orientations being aligned with the pattern (Figure 3.4). It can be assumed that neurites that grow in the direction of the pattern have a higher probability to develop into axons than unaligned neurites. The effect of topographical guidance and alignment diminished as the diameter and pitch increased (A1 and A2 substrates), in line with previous studies (Mattotti et al. 2015; Kundu et al. 2013). Although, similar responses have been reported in previous studies on both isotropic and anisotropic substrates (Walsh et al. 2005; Repić et al. 2016), it is very difficult to compare results from different studies due to the use of different materials, shapes, dimensions, and methods of measurement. However, most of the studies report that periodic structural features increase axonal lengths. Moreover, such features tended to induce axon alignment to the presented pattern. It appears that a growth cone follows existing cues while exploring its surroundings but if a new cue such as a neighboring pillar is close enough, it will extend to that cue. This behavior would result in axon alignment to the direction of the pattern since pillars act as geometrical constraints providing directional guidance.

4.3. Neuronal development on 400 nm high nanopillars

The second group of substrates had pillars with the same diameter and pitch as the first group while being 4 times higher (400 nm). These substrates showed a significantly stronger increase in axon length and alignment and a decrease in neurite number (Figure 3.6.A, C, D, Figure 3.7.). This effect was easily observable on the fluorescent images (Figure 3.5), which showed long axons growing strictly in the direction of the pattern. The soma area was decreased on substrates with pillars of larger diameters (B1, B2). Since PLL coating improves adhesion by unspecific electrostatic interaction with the cell membrane without being involved in chemical signaling, it is assumed that these changes in the soma area are due to topography. Nanostructured substrates have a discontinuous surface that could lead to a smaller soma area in comparison to the flat surface. The nanostructures possibly act as geometrical constraints and reduce the contact area between the surface and the cell.

Several studies dealt with the influence of feature height on neuronal growth and guidance. Baranes et al. (2012) showed that topographic cues as low as 10 nm can influence neuronal growth while Chua et al. (2014) demonstrated that neurite elongation, alignment and neuronal differentiation were increased with increasing depth of gratings. Furthermore, it seems that an increase in diameter and spacing of the 400 nm pillars does not decrease the axon length and alignment to the pattern as was observed on the 100 nm pillars. It is assumed that pillars act as anchoring points for the growth cone that reduce the frequency of protrusion-retraction events and promote accelerated neurite growth. Since the only difference between the 100 nm pillars and 400 nm pillars is their height, one can assume that higher pillars present stronger cues possibly due to their increased surface area and further promote neurite growth and guidance.

4.4. Dynamics of neuronal development on nanostructured substrates

Time-lapse microscopy enables investigation of the influence of different structural confinements on the dynamics of neuronal development. Neurons cultured on topographies show a more directional and efficient growth (Figure 3.8.B). Furthermore, MSD analysis shows that growth cones on nanostructured substrates explored a larger area in comparison to those on flat surfaces (Figure 3.9.A, B). This, in combination with a higher directionality, resulted in a larger net

displacement, i.e. longer axons. These findings correspond well to the assumption that pillars act as anchoring points for the growth cone whereby they reduce the frequency of protrusion and retraction events making the growth more efficient. The mechanisms of the accelerated neurite growth induced by topographies is still unknown but one could hypothesize that the spacing between contact sites i.e. pillars causes neurite tension which could lead to neurite stretching and accelerated outgrowth. Furthermore, periodic actin rings observed in axons could play a role in sustaining these mechanical strains (Xu et al. 2013). Bugnicourt et al. (2014) observed discrete actin/vinculin structures that could relate to adhesion complexes and whose spacing could have been imposed by the distance between the pillars. Therefore, these adhesion complexes could mediate an increase in neurite tension resulting in accelerated outgrowth.

4.5. Mechanisms of topography-induced responses

Despite great advances in nanotechnology and fabrication techniques, the basic mechanisms by which cells respond to physical cues remain obscure. Gertz et al. (2010) demonstrated that actin filaments assemble into networks in the shape of the underlying topography. Additionally, local actin instability was shown to be a determining factor in axon development (Bradke and Dotti 1999) and it could be possible that this instability is caused by nanotopography, thus promoting neurite growth and alignment. In this study, cortical neurons were successfully transfected with a fluorescent actin marker, Lifeact-RFP. This 17-amino-acid peptide does not interfere with actin dynamics *in vivo* or *in vitro,* making it suitable for investigation of actin dynamics in real time. It was shown that the transfection efficiency (~20%) and viability (~10%) was sufficient to collect enough data and the live cell imaging setup was optimized to ensure minimal phototoxicity with cells surviving long term imaging (>3 DIV). Time-lapse imaging showed that cortical neurons enter Stage 3 of their development when one neurite breaks the overall symmetry and starts growing rapidly ~12 hours after seeding. Since the fluorescent signal from the actin binding protein could be detected 10-12 hours after seeding and it was constitutively expressed for >3 DIV it would be possible to study actin dynamics during axon formation in response to topography. The thickness of the substrates prevented time-lapse imaging with high resolution since it exceeded the working distance of the high resolution immersion objectives. A possible approach would be to

use wafers of lower thickness for replication since the thickness of the polymer layer itself is <500 nm.

5. CONCLUSION

All OrmoComp polymer substrates supported neuronal growth and development without any significant detrimental effects on cell viability. Both nano- and microscale pillars promoted neurite growth and alignment to the underlying pattern, an effect that diminished with increasing pillar diameter and spacing. Moreover, an increase in pillar height greatly enhanced the axon guiding effect resulting in longer and more aligned axons. Time-lapse imaging revealed that axons growing on different topographies explored a larger area and had a more rapid and directional growth which resulted in the observed increase in axon length.

This study demonstrates the suitability of OrmoComp nano- and micropillar substrates for supporting and controlling growth of cortical neurons. Such surfaces could be used in creating a well-organized neuronal network and possibly allow for neuronal stimulation and electrical measurement of signals arising from single cells in a structured network. In addition to their applicability in micro-electrode arrays, topographies that promote axon growth and guidance are promising for tissue engineering applications, especially as supporting scaffolds in nerve regeneration after injury.

Therefore, this study lays a foundation for gaining a better understanding of the molecular mechanisms that regulate the neuronal responses to topographical cues and is a step towards a more rational approach in the design of novel platforms for controlling neuronal growth and development.

6. LITERATURE

Avellino, A. M., Hart, D., Dailey, A. T., MacKinnon, M., Ellegala, D. and Kliot, M. (1995) Differential macrophage responses in the peripheral and central nervous system during wallerian degeneration of axons. Experimental Neurology. **136(2)**, 183–198.

Baranes, K., Chejanovsky, N., Alon, N., Sharoni, A. and Shefi, O. (2012) Topographic cues of nano-scale height direct neuronal growth pattern. Biotechnology and Bioengineering. **109(7)**, 1791–1797.

Becker, C. G. and Becker, T. (2007) Growth and pathfinding of regenerating axons in the optic projection of adult fish. Journal of Neuroscience Research. **85(12)**, 2793–2799.

Bellamkonda, R. V (2006) Peripheral nerve regeneration: an opinion on channels, scaffolds and anisotropy. Biomaterials. **27(19)**, 3515–3518.

Bernhardt, R. R. (1999) Cellular and molecular bases of axonal pathfinding during embryogenesis of the fish central nervous system. Journal of Neurobiology. **38(1)**, 137–160.

Bettinger, C. J., Langer, R. and Borenstein, J. T. (2009) Engineering Substrate Topography at the Micro- and Nanoscale to Control Cell Function. Angewandte Chemie International Edition. **48(30)**, 5406–5415.

Biswas, A., Bayer, I. S., Biris, A. S., Wang, T., Dervishi, E. and Faupel, F. (2012) Advances in top–down and bottom–up surface nanofabrication: Techniques, applications & future prospects. Advances in Colloid and Interface Science. **170(1–2)**, 2–27.

den Braber, E. T., de Ruijter, J. E., Ginsel, L. A., von Recum, A. F. and Jansen, J. A. (1996) Quantitative analysis of fibroblast morphology on microgrooved surfaces with various groove and ridge dimensions. Biomaterials. **17(21)**, 2037–2044.

den Braber, E. T., de Ruijter, J. E., Ginsel, L. A., von Recum, A. F. and Jansen, J. A. (1998) Orientation of ECM protein deposition, fibroblast cytoskeleton, and attachment complex components on silicone microgrooved surfaces. Journal of biomedical materials research. **40(2)**, 291–300.

Bradke, F. and Dotti, C. G. (1999) The role of local actin instability in axon formation. Science. **283(5409)**, 1931–1934.

Braeken, D., Huys, R., Loo, J., Bartic, C., Borghs, G., Callewaert, G. and Eberle, W. (2010) Localized electrical stimulation of in vitro neurons using an array of sub-cellular sized electrodes. Biosensors & bioelectronics. **26(4),** 1474–1477.

Bugnicourt, G., Brocard, J., Nicolas, A. and Villard, C. (2014) Nanoscale surface topography reshapes neuronal growth in culture. Langmuir : the ACS journal of surfaces and colloids. **30(15)**, 4441–4449.

Bunge, R. P. (1994) The role of the Schwann cell in trophic support and regeneration. Journal of neurology. **242(1)**, S19-21.

Butler, S. J. and Tear, G. (2007) Getting axons onto the right path: the role of transcription factors in axon guidance. Development. **134(3)**, 439–448.

Case, L. B. and Waterman, C. M. (2015) Integration of actin dynamics and cell adhesion by a three-dimensional, mechanosensitive molecular clutch. Nature Cell Biology. **17(8)**, 955–963.

Chen, C. S., Alonso, J. L., Ostuni, E., Whitesides, G. M. and Ingber, D. E. (2003) Cell shape provides global control of focal adhesion assembly. Biochemical and Biophysical Research Communications. **307(2)**, 355–361.

Chen, C. S., Jiang, X. and Whitesides, G. M. (2005) Microengineering the Environment of Mammalian Cells in Culture. MRS Bulletin. **30(3)**, 194–201.

Chen, Y. (2015) Nanofabrication by electron beam lithography and its applications: A review. Microelectronic Engineering, **135**, 57–72.

Chilton, J. K. (2006) Molecular mechanisms of axon guidance. Developmental biology. **292(1)**, 13–24.

Cho, W. K., Kang, K., Kang, G., Jang, M. J., Nam, Y. and Choi, I. S. (2010) Pitch-dependent acceleration of neurite outgrowth on nanostructured anodized aluminum oxide substrates. Angewandte Chemie (International ed. in English). **49(52)**, 10114–10118.

Choi, C. K., Vicente-Manzanares, M., Zareno, J., Whitmore, L. A., Mogilner, A. and Horwitz, A.

R. (2008) Actin and α-actinin orchestrate the assembly and maturation of nascent adhesions in a myosin II motor-independent manner. Nature cell biology. **10(9)**, 1039–1050.

Chou, S. Y., Krauss, P. R. and Renstrom, P. J. (1996) Nanoimprint lithography. Journal of Vacuum Science & Technology B: Microelectronics and Nanometer Structures. **14(6)**, 4129.

Chua, J. S., Chng, C. P., Moe, A. A. K., Tann, J. Y., Goh, E. L. K., Chiam, K. H. and Yim, E. K. F. (2014) Extending neurites sense the depth of the underlying topography during neuronal differentiation and contact guidance. Biomaterials.

Clark, P., Connolly, P., Curtis, A. S., Dow, J. A. and Wilkinson, C. D. (1991) Cell guidance by ultrafine topography in vitro. Journal of cell science. **99** (Pt 1), 73–77.

Cukierman, E., Pankov, R., Stevens, D. R. and Yamada, K. M. (2001) Taking Cell-Matrix Adhesions to the Third Dimension. Science. **294(5547)**, 1708 LP-1712.

Dalby, M. J., Riehle, M. O., Sutherland, D. S., Agheli, H. and Curtis, A. S. G. (2004) Fibroblast response to a controlled nanoenvironment produced by colloidal lithography. Journal of Biomedical Materials Research Part A. **69A(2)**, 314–322.

Dent, E. W. and Gertler, F. B. (2003) Cytoskeletal dynamics and transport in growth cone motility and axon guidance. Neuron. **40(2)**, 209–227.

Dotti, G., Sullivan, A., Biology, C., College, A. M. and York, N. (1988) The Establishment of Polarity by Hippocampal. (April).

Dowell-Mesfin, N. M., Abdul-Karim, M.-A., Turner, A. M. P., Schanz, S., Craighead, H. G., Roysam, B., Turner, J. N. and Shain, W. (2004) Topographically modified surfaces affect orientation and growth of hippocampal neurons. Journal of neural engineering. **1(2)**, 78–90.

Dunn, G. A. and Brown, A. F. (1986) Alignment of fibroblasts on grooved surfaces described by a simple geometric transformation. Journal of cell science. **83**, 313–340.

Flemming, R. G., Murphy, C. J., Abrams, G. A., Goodman, S. L. and Nealey, P. F. (1999) Effects of synthetic micro- and nano-structured surfaces on cell behavior. Biomaterials. **20(6)**, 573–588.

Fluitman, H. J. and H. G. and M. de B. and M. E. and J. (1996) A survey on the reactive ion etching of silicon in microtechnology. Journal of Micromechanics and Microengineering. **6(1)**, 14.

Foley, J. D., Grunwald, E. W., Nealey, P. F. and Murphy, C. J. (2005) Cooperative modulation of neuritogenesis by PC12 cells by topography and nerve growth factor. Biomaterials. **26**(**17**), 3639–3644.

Forscher, P. and Smith, S. J. (1988) Actions of cytochalasins on the organization of actin filaments and microtubules in a neuronal growth cone. Journal of Cell Biology. **107(4)**, 1505–1516.

Frey, M. T., Tsai, I. Y., Russell, T. P., Hanks, S. K. and Wang, Y.-L. (2006) Cellular responses to substrate topography: role of myosin II and focal adhesion kinase. Biophysical journal. **90(10)**, 3774–3782.

Geller, H. M. and Fawcett, J. W. (2002) Building a Bridge: Engineering Spinal Cord Repair. Experimental Neurology. **174(2)**, 125–136.

Gerecht, S., Bettinger, C. J., Zhang, Z., Borenstein, J. T., Vunjak-Novakovic, G. and Langer, R. (2007) The effect of actin disrupting agents on contact guidance of human embryonic stem cells. Biomaterials. **28**(**28**), 4068–4077.

Gertz, C. C., Leach, M. K., Birrell, L. K., Martin, D. C., Feldman, E. L. and Corey, J. M. (2010) Accelerated neuritogenesis and maturation of primary spinal motor neurons in response to nanofibers. Developmental Neurobiology. **70(8)**, 589–603.

Goldberg, J. L. (2003) How does an axon grow? Genes & development. **17(8)**, 941–958.

Gomez, T. M. and Letourneau, P. C. (2014) Actin dynamics in growth cone motility and navigation. Journal of Neurochemistry **129(2)**, 221–234.

Gorelik, R. and Gautreau, A. (2014) Quantitative and unbiased analysis of directional persistence in cell migration. Nature Protocols. **9(8)**, 1931–1943.

Govek, E., Newey, S. E. and Aelst, L. Van (2005) The role of the Rho GTPases in neuronal development The role of the Rho GTPases in neuronal development. Genes and Development. **19**, 1–49.

Hammarback, J. A. and Letourneau, P. C. (1986) Neurite extension across regions of low cell-substratum adhesivity: implications for the guidepost hypothesis of axonal pathfinding. Developmental biology. **117(2)**, 655–662.

Hanson, J. N., Motala, M. J., Heien, M. L., Gillette, M., Sweedler, J. and Nuzzo, R. G. (2009) Textural guidance cues for controlling process outgrowth of mammalian neurons. Lab on a chip. **9(1)**, 122–131.

Harrison, R. G. (1912) The cultivation of tissues in extraneous media as a method of morpho-genetic study. The Anatomical Record. **6(4)**, 181–193.

Hatsopoulos, N. and Donoghue, J. (2009) The science of neural interface systems. Annual review of neuroscience. **32**, 249–266.

Hirono, T., Torimitsu, K., Kawana, A. and Fukuda, J. (1988) Recognition of artificial microstructures by sensory nerve fibers in culture. Brain research. **446(1)**, 189–194.

Humphries, J. D., Wang, P., Streuli, C., Geiger, B., Humphries, M. J. and Ballestrem, C. (2007) Vinculin controls focal adhesion formation by direct interactions with talin and actin. **179(5)**, 1043–1057.

Hynes, R. O. (2002) Integrins: bidirectional, allosteric signaling machines. Cell. **110(6)**, 673–687.

Izzard, C. S. (1988) A precursor of the focal contact in cultured fibroblasts. Cell motility and the cytoskeleton. **10(1–2)**, 137–142.

Jacobson, C., Schnapp, B. and Banker, G. A. (2006) A Change in the Selective Translocation of the Kinesin-1 Motor Domain Marks the Initial Specification of the Axon. 797–804.

Johansson, F., Carlberg, P., Danielsen, N., Montelius, L. and Kanje, M. (2006) Axonal outgrowth on nano-imprinted patterns. Biomaterials. **27(8)**, 1251–1258.

Joo, S., Yeon Kim, J., Lee, E., Hong, N., Sun, W., Nam, Y., Gage, F. H., Doetsch, F., Lathia, J. D., Saha, K., Leipzig, N. D., Shoichet, M. S., Bakhru, S., Beduer, A., Kim, W. R., Jang, M. J., Joo, S., Sun, W., Nam, Y., Ricoult, S. G., Thompson-Steckel, G., Correia, J. P., Kennedy, T. E., Juncker, D., Tanaka, N., Yang, I. H., Co, C. C., Ho, C. C., Joo, S., Kang, K., Nam, Y., Rana, K., Timmer, B. J., Neeves, K. B., Tourovskaia, A., Dertinger, S. K., Jiang, X., Li, Z., Murthy, V. N., Whitesides, G. M., Millet, L. J., Stewart, M. E., Nuzzo, R. G., Gillette, M. U., Ruiz, A., Magnusson, A. K., Linderholm, P., Vieider, C., Ulfendahl, M., Erlandsson, A., Konagaya, S., Kato, K., Nakaji-Hirabayashi, T., Arima, Y., Iwata, H., Wang, Y., Xu, Z., Kam, L. C., Shi, P., Shen, Q., Gao, F. B., Raff, M., Gross, R. E., Qian, X., Davis, A. A., Goderie, S. K., Temple, S.,

Gaiano, N., Nye, J. S., Fishell, G., Lu, Q. R., Zhou, Q., Wang, S., Anderson, D. J., Cau, E., Gradwohl, G., Fode, C., Guillemot, F., Kageyama, R., Ishibashi, M., Takebayashi, K., Tomita, K., Nieto, M., Schuurmans, C., Britz, O., Guillemot, F., Taupin, P., Dityatev, A., Seidenbecher, C. I., Schachner, M., Anton, E., Andrada, E. C., Lanari, A., Esch, T., Lemmon, V., Banker, G., Ricoult, S. G., Goldman, J. S., Stellwagen, D., Juncker, D., Kennedy, T. E., Philipsborn, A. C. von, Shi, P., Shen, K., Kam, L. C., Soares, S., Sotelo, C., Wang, X., Sohn, J., Benner, E. J., Silver, J., Miller, J. H., Cho, H. M., Kim, J. Y., Kim, H. and Sun, W. (2015) Effects of ECM protein micropatterns on the migration and differentiation of adult neural stem cells. Scientific Reports. **5**(April), 13043.

Kang, K., Choi, S.-E., Jang, H. S., Cho, W. K., Nam, Y., Choi, I. S. and Lee, J. S. (2012) In vitro developmental acceleration of hippocampal neurons on nanostructures of self-assembled silica beads in filopodium-size ranges. Angewandte Chemie (International ed. in English). **51(12)**, 2855–2858.

Kang, K., Yoon, S. Y., Choi, S.-E., Kim, M.-H., Park, M., Nam, Y., Lee, J. S. and Choi, I. S. (2014) Cytoskeletal Actin Dynamics are Involved in Pitch-Dependent Neurite Outgrowth on Bead Monolayers. Angewandte Chemie International Edition. **53(24)**, 6075–6079.

Käpylä, E., Sorkio, A., Teymouri, S., Lahtonen, K., Vuori, L., Valden, M., Skottman, H., Kellomäki, M. and Juuti-Uusitalo, K. (2014) Ormocomp-Modified Glass Increases Collagen Binding and Promotes the Adherence and Maturation of Human Embryonic Stem Cell-Derived Retinal Pigment Epithelial Cells. Langmuir. American Chemical Society. **30(48),** 14555–14565.

Keefer, E. W., Botterman, B. R., Romero, M. I., Rossi, A. F. and Gross, G. W. (2008) Carbon nanotube coating improves neuronal recordings. Nature Nanotechnology. **3(7)**, 434–439.

Kim, D. H., Provenzano, P. P., Smith, C. L. and Levchenko, A. (2012) Matrix nanotopography as a regulator of cell function. Journal of Cell Biology. **197(3)**, 351–360.

Konrad, P. and Shanks, T. (2010) Implantable brain computer interface: Challenges to neurotechnology translation. Neurobiology of Disease. **38(3)**, 369–375.

Kshitiz, Afzal, J., Kim, S.-Y. and Kim, D.-H. (2015) A nanotopography approach for studying the structure-function relationships of cells and tissues. Cell Adhesion & Migration. **9(4)**, 300–307.

Kundu, A., Micholt, L., Friedrich, S., Rand, D. R., Bartic, C., Braeken, D. and Levchenko, A.

(2013) Superimposed topographic and chemical cues synergistically guide neurite outgrowth. Lab on a chip. **13(15)**, 3070–3081.

Lei, P., Ayton, S., Finkelstein, D. I., Adlard, P. A., Masters, C. L. and Bush, A. I. (2010) Tau protein: Relevance to Parkinson's disease. The International Journal of Biochemistry & Cell Biology. **42(11)**, 1775–1778.

Letourneau, P. C. (1979) Cell-substratum adhesion of neurite growth cones, and its role in neurite elongation. Experimental Cell Research. **124(1)**, 127–138.

Li, S., Guan, J.-L. and Chien, S. (2005) Biochemistry and biomechanics of cell motility. Annual Review of Biomedical Engineering. **7**, 105–150.

Lietz, M., Dreesmann, L., Hoss, M., Oberhoffner, S. and Schlosshauer, B. (2006) Neuro tissue engineering of glial nerve guides and the impact of different cell types. Biomaterials. **27(8)**, 1425–1436.

Lowery, L. A. and Van Vactor, D. (2009) The trip of the tip: understanding the growth cone machinery. Nature reviews. Molecular cell biology. **10(5)**, 332–43.

Ma, P. X. (2008) Biomimetic Materials for Tissue Engineering. Advanced Drug Delivery Reviews. 184–198.

Ma, W., Tavakoli, T., Derby, E., Serebryakova, Y., Rao, M. S. and Mattson, M. P. (2008) Cell-extracellular matrix interactions regulate neural differentiation of human embryonic stem cells. BMC Developmental Biology. **8**, 90.

Mahoney, M. J., Chen, R. R., Tan, J. and Saltzman, W. M. (2005) The influence of microchannels on neurite growth and architecture. Biomaterials. **26(7)**, 771–778.

Martinez, E., Engel, E., Planell, J. A. and Samitier, J. (2009) Effects of artificial micro- and nano-structured surfaces on cell behaviour. Annals of Anatomy. **191(1)**, 126–135.

Mattotti, M., Micholt, L., Braeken, D. and Kovacic, D. (2015) Characterization of spiral ganglion neurons cultured on silicon micro-pillar substrates for new auditory neuro-electronic interfaces. Journal of Neural Engineering. **12(2)**, 26001.

Meyle, J., Wolburg, H. and von Recum, A. F. (1993) Surface micromorphology and cellular

interactions. Journal of Biomaterials Applications. **7(4)**, 362–374.

Mitchison, T. J. and Cramer, L. P. (1996) Actin-based cell motility and cell locomotion. Cell. **84(3)**, 371–379.

Mitchison, T. and Kirschner, M. (1988) Cytoskeletal dynamics and nerve growth. Neuron. **1(9)**, 761–772.

Mitra, S. K., Hanson, D. A. and Schlaepfer, D. D. (2005) Focal adhesion kinase: in command and control of cell motility. Nature Reviews. Molecular Cell Biology. **6(1)**, 56–68.

Nadarajah, B., Alifragis, P., Wong, R. O. L. and Parnavelas, J. G. (2002) Ventricle-directed migration in the developing cerebral cortex. Nature neuroscience. **5(3)**, 218–224.

Nagata, I., Kawana, A. and Nakatsuji, N. (1993) Perpendicular contact guidance of CNS neuroblasts on artificial microstructures. Development. **117(1)**, 401–408.

Nagata, I., Ono, K., Kawana, A. and Kimura-Kuroda, J. (2006) Aligned neurite bundles of granule cells regulate orientation of Purkinje cell dendrites by perpendicular contact guidance in two-dimensional and three-dimensional mouse cerebellar cultures. The Journal of Comparative Neurology. **499(2)**, 274–289.

Nasrollahi, S., Banerjee, S., Qayum, B., Banerjee, P. and Pathak, A. (2016) Nano-scale matrix topography influences micro-scale cell motility through adhesions, actin organization, and cell shape. ACS Biomaterials Science & Engineering.

Ning, D., Duong, B., Thomas, G., Qiao, Y., Ma, L., Wen, Q. and Su, M. (2016) Mechanical and Morphological Analysis of Cancer Cells on Nanostructured Substrates. Langmuir.

Ono, K. and Kawamura, K. (1989) Migration of immature neurons along tangentially oriented fibers in the subpial part of the fetal mouse medulla oblongata. Experimental brain research. **78(2)**, 290–300.

Ono, K., Shokunbi, T., Nagata, I., Tokunaga, A., Yasui, Y. and Nakatsuji, N. (1997) Filopodia and growth cones in the vertically migrating granule cells of the postnatal mouse cerebellum. Experimental brain research. **117(1)**, 17–29.

Provenzano, P. P., Inman, D. R., Eliceiri, K. W., Trier, S. M. and Keely, P. J. (2008) Contact

guidance mediated three-dimensional cell migration is regulated by Rho/ROCK-dependent matrix reorganization. Biophysics Journal. **95(11)**, 374–5384.

Rajnicek, A., Britland, S. and McCaig, C. (1997) Contact guidance of CNS neurites on grooved quartz: influence of groove dimensions, neuronal age and cell type. Journal of Cell Science. **110** (Pt 2), 2905–2913.

Rajnicek, A. and McCaig, C. (1997) Guidance of CNS growth cones by substratum grooves and ridges: effects of inhibitors of the cytoskeleton, calcium channels and signal transduction pathways. Journal of Cell Science. **110** (Pt 2), 2915–2924.

Rakic, P. (1972) Mode of cell migration to the superficial layers of fetal monkey neocortex. The Journal of Comparative Neurology. **145(1)**, 61–83.

Repić, T., Madirazza, K., Bektur, E. and Sapunar, D. (2016) Characterization of dorsal root ganglion neurons cultured on silicon micro-pillar substrates. Scientific Reports. **6**, 39560.

Riveline, D., Zamir, E., Balaban, N. Q., Schwarz, U. S., Ishizaki, T., Narumiya, S., Kam, Z., Geiger, B. and Bershadsky, A. D. (2001) Focal contacts as mechanosensors: externally applied local mechanical force induces growth of focal contacts by an mDia1-dependent and ROCK-independent mechanism. The Journal of Cell Biology. **153(6)**, 1175–1186.

Roskams, A. J. I., Cai, X. and Ronnett, G. V (1998) Expression of neuron-specific beta-III tubulin during olfactory neurogenesis in the embryonic and adult rat. Neuroscience. **83(1)**, 191–200.

Sanford, S. D., Gatlin, J. C., Hokfelt, T. and Pfenninger, K. H. (2008) Growth cone responses to growth and chemotropic factors. The European Journal of Neuroscience. **28(2)**, 268–278.

Schizas, C. and Karalekas, D. (2011) Mechanical characteristics of an Ormocomp((R)) biocompatible hybrid photopolymer. Journal of the Mechanical Behavior of Biomedical Materials. **4(1)**, 99–106.

da Silva, J. S. and Dotti, C. G. (2002) Breaking the neuronal sphere: regulation of the actin cytoskeleton in neuritogenesis. Nature Reviews. Neuroscience. **3(9)**, 694–704.

Spedden, E., Wiens, M. R., Demirel, M. C. and Staii, C. (2014) Effects of surface asymmetry on neuronal growth. PLoS ONE. **9(9)**.

Teixeira, A. I., Abrams, G. A., Bertics, P. J., Murphy, C. J. and Nealey, P. F. (2003) Epithelial contact guidance on well-defined micro- and nanostructured substrates. Journal of Cell Science. **116(10)**, 1881–1892.

Tessier-Lavigne, M. and Goodman, C. S. (1996) The molecular biology of axon guidance. Science. **274(5290)**, 1123–1133.

Walboomers, X. F., Monaghan, W., Curtis, A. S. G. and Jansen, J. A. (1999) Attachment of fibroblasts on smooth and microgrooved polystyrene. Journal of Biomedical Materials Research. **46(2)**, 212–220.

Walsh, J. F., Manwaring, M. E. and Tresco, P. A. (2005) Directional neurite outgrowth is enhanced by engineered meningeal cell-coated substrates. Tissue engineering. **11(7–8)**, 1085–1094.

Wang, Y., Botvinick, E. L., Zhao, Y., Berns, M. W., Usami, S., Tsien, R. Y. and Chien, S. (2005) Visualizing the mechanical activation of Src. Nature. **434(7036)**, 1040–1045.

Wojciak-Stothard, B., Curtis, A., Monaghan, W., MacDonald, K. and Wilkinson, C. (1996) Guidance and activation of murine macrophages by nanometric scale topography. Experimental cell research. **223(2)**, 426–435.

Wojciak-Stothard, B., Curtis, A. S., Monaghan, W., McGrath, M., Sommer, I. and Wilkinson, C. D. (1995) Role of the cytoskeleton in the reaction of fibroblasts to multiple grooved substrata. Cell Motility and the Cytoskeleton. **31(2)**, 147–158.

Xu, K., Zhong, G. and Zhuang, X. (2013) Actin, spectrin, and associated proteins form a periodic cytoskeletal structure in axons. Science. **339(6118)**, 452–456.

Yamada, K. M. and Cukierman, E. (2017) Modeling Tissue Morphogenesis and Cancer in 3D. Cell. Elsevier. **130(4)**, 601–610.

Yao, L., Wang, S., Cui, W., Sherlock, R., O'Connell, C., Damodaran, G., Gorman, A., Windebank, A. and Pandit, A. (2009) Effect of functionalized micropatterned PLGA on guided neurite growth. Acta Biomaterialia. **5(2)**, 580–588.

Zaidel-Bar, R., Cohen, M., Addadi, L. and Geiger, B. (2004) Hierarchical assembly of cell–matrix adhesion complexes. Biochemical Society Transactions. **32(3)**, 416 LP-420.

Zamir, E. and Geiger, B. (2001) Molecular complexity and dynamics of cell-matrix adhesions. Journal of Cell Science. **114**(Pt 20), 3583–3590.

Zou, Y. and Lyuksyutova, A. I. (2007) Morphogens as conserved axon guidance cues. Current Opinion in Neurobiology. **17(1)**, 22–28.

7. CURRICULUM VITAE

I was born on January 2nd, 1993, in Split, Croatia. In 2011, I enrolled into the Undergraduate study of Molecular biology at the Faculty of Science, University of Zagreb. During that time, I participated in the "Night of Biology" for which I received a Special Rector's award in 2012. On the third year of my undergraduate studies I conducted a laboratory practice in the field of biochemistry under the supervision of dr. Ita Gruić, Prof. In 2014, I enrolled into the Graduate study of Molecular biology. During the summer of 2015, I participated in the International School of Biophysics and Soft Matter during which I worked in the Center of Advanced European Studies and Research in Bonn, Germany under the supervision of dr. Shatanik Mukherjee in the field of protein structural dynamics. From April, 2016 to March, 2017 I conducted my graduation thesis research in Forschungszentrum Juelich, Germany under the supervision of dr. Dirk Mayer.